Tectonophysics 857 (2023) 229841

Contents lists available at ScienceDirect

Tectonophysics

journal homepage: www.elsevier.com/locate/tecto

Contrasting thermal histories in the Dom Feliciano Belt triggered by magmatism related to the Paraná-Etendeka LIP and fracture zone proximity

Edgar do Amaral Santos [a,*], Andréa Ritter Jelinek [b], Daniel Stockli [c], Frederico Antônio Genezine [d]

[a] Programa de Pós-Graduação em Geociências, Universidade Federal do Rio Grande do Sul, Brazil
[b] Instituto de Geociências, Universidade Federal do Rio Grande do Sul, Brazil
[c] University of Texas at Austin, United States of America
[d] Instituto de Pesquisas Energéticas e Nucleares, Centro do Reator de Pesquisas, Brazil

ARTICLE INFO

Keywords:
Thermochronology
Dom Feliciano Belt
Apatite (U—Th)/He
Apatite fission track
Low-Temperature Thermochronology

ABSTRACT

The present-day southern Brazilian continental margin rests on top of the Dom Feliciano Belt (DFB) and adjacent cratons. This belt formed through the collision of the Rio de La Plata, Kalahari, Paranapanema, Congo and Luis Alves paleoplates in the Neoproterozoic. Several low-temperature thermochronology works were executed in the area, although none of them demonstrated how the basement temperature of the entire DFB evolved through time. To this end, this work aims to provide new Apatite Fission Track (AFT) and Apatite (U—Th)/He (AHe) ages for samples collected in the Catarinense Shield, in the northern DFB, and to perform inverse modeling in those samples. Besides, the collection of the basement temperature of 128 locations across the entire belt and adjacent cratons provided thermal information to create inverse-distance weighted interpolation maps documenting the progression of the temperature from 360 to 30 Ma. New AFT ages range from 126.6 ± 24.1 to 60.3 ± 6.03 Ma, whereas AHe ages span from 153.0 ± 9.2 to 62.5 ± 3.7 Ma. Mean track lengths are short to medium, suggesting complete thermal annealing of apatite crystals. Apatite single-grain eU concentration range from 4.5 to 96 μg/g and display a sparse correlation with AHe ages. Interpolation maps evidence a contrasting temperature evolution of the northern DFB and bordering cratons relative to the southern segment and surrounding cratons. Near-surface exposure of the basement in the northern segment was possibly much earlier than in the south, followed by partial burial by the sedimentary successions of the Paraná Basin. The emplacement of volcanic rocks of the Paraná-Etendeka Large Igneous Province and associated dyke swarms and alkaline volcanic plugs related to the Florianópolis Fracture Zone raised and sustained higher basement temperatures until 30 Ma, resetting low-temperature thermochronometers in the northern DFB, which was minor to absent in the southern DFB.

1. Introduction

Before the opening of the South Atlantic Ocean during the Cretaceous, the southern continental margin of Brazil was in an intracontinental setting. The continent's interior was formed by several terranes of Archean to Proterozoic ages that were contiguous, such as the Rio de La Plata, Kalahari, Paranapanema, Congo, and Luis Alves cratons, forming the Dom Feliciano mobile belt during the Neoproterozoic and composing the West Gondwana paleocontinent (Basei et al., 2008; Hasui, 2010; Oriolo et al., 2017). The continent interior also recorded pulses of exhumation (Milani and De Wit, 2014), deposition of sedimentary successions (Milani et al., 2007a), magmatic and volcanic emplacement of igneous rocks (Stewart et al., 1996; Turner et al., 1994), and the rifting stages of the South Atlantic opening (Chang et al., 1992; Mohriak et al., 2008a). However, to this extent, it is not clear how the basement temperature of the entire Dom Feliciano Belt and adjacent cratons evolved in response to tectonic and magmatic processes during the Phanerozoic.

To investigate this question, we used two low-temperature thermochronometers to retrieve the ages and the thermal information of samples collected in the Catarinense Shield, located in the northern Dom Feliciano Belt, in southern Brazil. We present in this paper 13 new apatite fission track (AFT) ages, 30 single-grain apatite (U—Th)/He analyzes (AHe) and new thermal histories about this region through

* Corresponding author.
E-mail address: edgar.amaral@ufrgs.br (E. do Amaral Santos).

https://doi.org/10.1016/j.tecto.2023.229841
Received 6 September 2022; Received in revised form 29 March 2023; Accepted 30 March 2023
Available online 20 April 2023

model inversion (Gallagher, 2012). In addition, interpolation maps for assessing the basement temperature of the entire Dom Feliciano Belt and surrounding cratons during the last 360 Ma were generated using the inverse distance weighted technique after compiling thermal history information of 128 locations. Additionally, we inspected track lengths and AHe-related parameter. The new data presented in this study indicate complete thermal resetting of low-temperature thermochronometers from rifting to post-rifting coeval to post-rifting exhumation for samples located in the northern Dom Feliciano Belt. The data provided here also points to a complex thermal evolution for the Rio de La Plata and Luis Alves cratons as well as for the Dom Feliciano Belt, since there are multiple episodes of accelerated cooling as well as reheating episodes and slow cooling. Furthermore, several sources of heat seem to have raised the temperature of the northern Dom Feliciano Belt, which strongly contrasts with the southern segment of the belt.

2. Geological background

During the Brasiliano/Pan-African orogenic cycle in the Neoproterozoic to the Ordovician, several paleocontinents and microplates of Archean to Proterozoic ages interacted with each other forming the West Gondwana continent (de Almeida et al., 1981; Hasui, 2010; De Brito Neves and Fuck, 2013) (Fig. 1a). This process led to the formation of the Mantiqueira Province, which extends from Uruguay to eastern Brazil. The Dom Feliciano Belt corresponds to the southern segment of this province (Basei, 1985), which is limited by the Rio de La Plata craton and the Nico Perez Terrane to the southwest, the Luís Alves Craton to the north, the South Atlantic Ocean to the east, and the Paleo- to Mesozoic volcanosedimentary units of the Paraná Basin to the west (Hueck et al., 2018b) (Fig. 1b).

The Rio de La Plata Craton (RDLP) consists of voluminous granite-gneissic terrains and relics of supracrustal rocks of Paleoproterozoic age (2.2–2.1 Ga), metamorphosed under greenschist facies. The Piedra Alta Terrane corresponds to the main segment of the craton, whereas the Tandilla Terrane outcrops to a lesser extent (Fig. 1b) (Oyhantçabal et al., 2018a). The Nico Perez Terrane is subdivided into three blocks that outcrop in Uruguay and Brazil (Fig. 1b). These units are composed of orthogneisses, amphibolites, migmatites, mafic-ultramafic igneous rocks, and metasediments of Archean to Paleoproterozoic ages (e.g., Hartmann, 1998; Hartmann et al., 2001; Gaucher et al., 2011; Oriolo et al., 2016; Philipp et al., 2016; Oyhantçabal et al., 2018b). The Luís Alves Craton (LAC) (Fig. 1b), a microplate of Archean to Paleoproterozoic age, is composed of a tonalite-trondhjemite-granodiorite suite, mafic-ultramafic bodies and a few paragneisses metamorphosed under medium to high-grade metamorphic granulite (Basei et al., 1992, 1998). Additionally, Neoproterozoic units composed of volcanosedimentary basins and alkaline-peralkaline granitoids are found within the LAC (Passarelli et al., 2018).

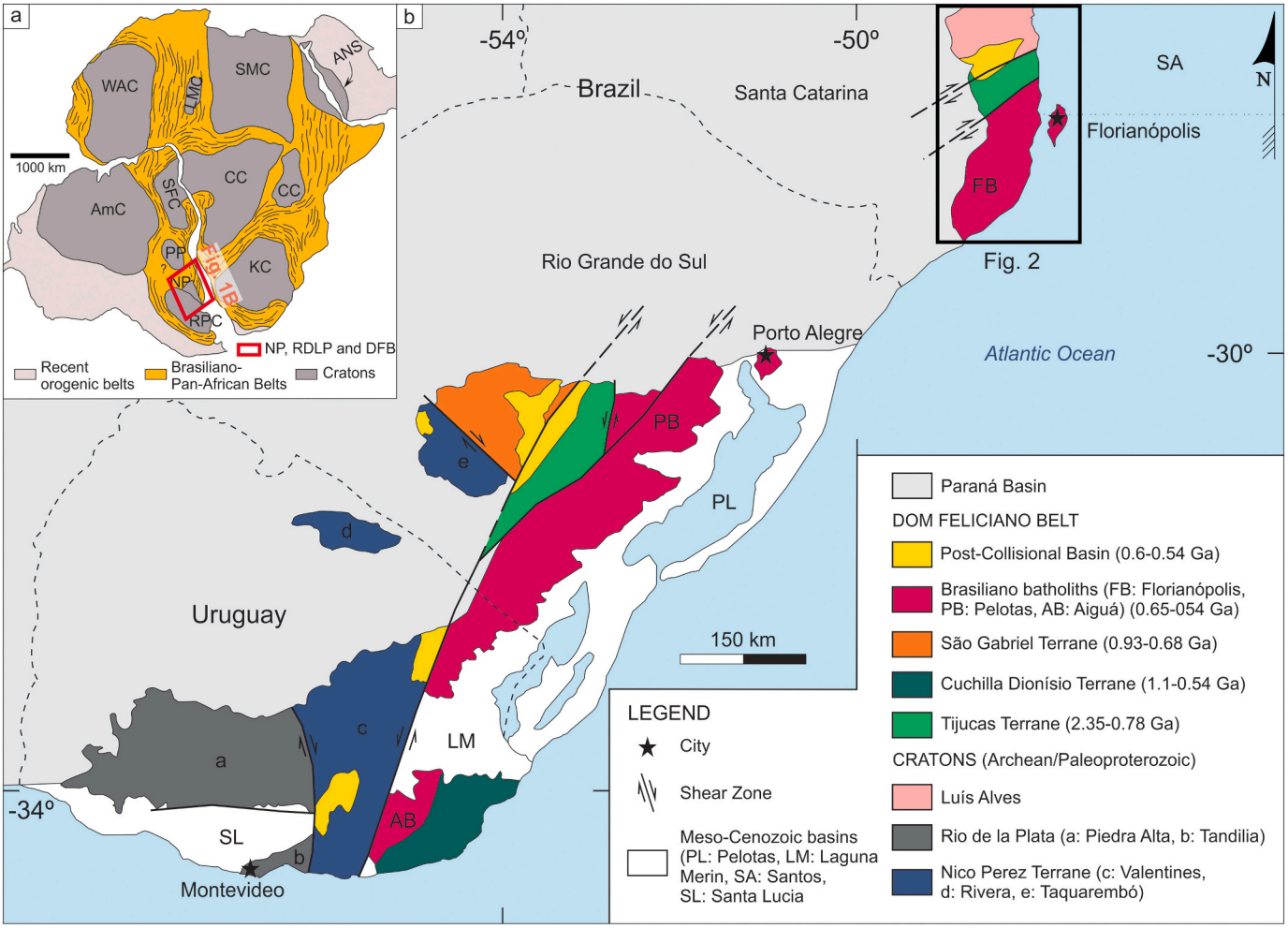

Fig. 1. a) West Gondwana map showing the cratonic nuclei, the belts formed in the Brasiliano/Pan-African event, and the recent orogenic belts (after Oriolo et al., 2017). Abbreviations are RDLP: Rio de La Plata Craton; NP: Nico Pérez Terrane; PP: Paranapanema Block; SFC: São Francisco Craton; AmC: Amazon Craton; KC: Kalahari Craton; CC: Congo Craton; LMC: Latea Metacraton; WAC: West Africa Craton; SMC: Sahara Metacraton; ANS: Arabian-Nubian Shield. b) The Dom Feliciano Belt and adjacent cratons along the continental margin of southern Brazil and Uruguay. After CPRM (2008) and Philipp et al. (2016).

The Dom Feliciano Belt (DFB) was assembled in the Neoproterozoic, during the Brasiliano/Pan-African orogenic cycle, when several terranes accreted, juxtaposed along shear zones (Philipp et al., 2016). In this context, the DFB is divided into four terranes and overlying sedimentary basins (Fig. 1b). The Cuchilla-Dionísio Terrane, also named Punta del Este Terrane, outcrops only in Uruguayan territory, and is composed of high-grade metamorphic rocks comprised by ortho- and para-derived granulites and migmatites of 800 and 770 Ma, with zircons containing metamorphic overgrowth of 650 Ma. The debate around this unit suggests it may correlate with orthogneisses of the Coastal Terrane in the Kaoko Belt (Basei et al., 2011; Oyhantçabal et al., 2011; Hueck et al., 2018b). The São Gabriel Terrane, located in southern Brazil, comprises two juvenile arcs and a late-collisional basin, along with records of ophiolite slivers. The older arc developed between 890 and 860 Ma, whereas the younger one evolved between 770 and 720 Ma (Philipp et al., 2018), recording the first stages of the Brasiliano/Pan-African cycle. The Tijucas Terrane encompasses basement inliers of Paleoproterozoic age, Statherian metagranites, Calymminian amphibolites, and Neoproterozoic metavolcano-sedimentary complexes (Philipp et al., 2016). The Neoproterozoic Brasiliano batholiths included in the DFB are named (i) Aiguá Batholith, in Uruguay; (ii) Pelotas Batholith on the border between Uruguay to the northeastern region of the Rio Grande do Sul State in Brazil; and (iii) Florianópolis Batholith in the Santa Catarina State in Brazil (Fig. 1b). These batholiths were generated during and after the Dom Feliciano orogeny and emplaced along high-angle transcurrent shear zones (Philipp et al., 2016). The suites are composed of high-K calc-alkaline granitoids with metaluminous to peraluminous affinity and most intrusions were emplaced between 650 and 550 Ma (Philipp et al., 2016; Philipp and Machado, 2005). Late to post-collisional basins resting on top of the DFB are composed of volcanosedimentary successions dated between 600 and 540 Ma (Paim and Chemale Jr, 2000; Guadagnin et al., 2010), such as the Camaquã and Itajaí basins in Brazil, and Arroyo del Soldado Group in Uruguay. The Archean to Neoproterozoic terranes in Uruguay, Rio Grande do Sul and Santa Catarina are, respectively, named Uruguayan Shield, Sul-Rio-Grandense Shield (SRGS), and Catarinense Shield.

The compressional stresses that promoted the assembly of Gondwana ceased during the Paleozoic, which allowed the erosion and deposition of sediments, forming intracontinental basins. The Paraná Basin is one of these depocenters, composed of a volcanosedimentary package divided into six supersequences formed during the Paleozoic to the Mesozoic and reaching a thickness of nearly 7 km (Milani et al., 2007a). To the west of the study area (Fig. 2), the emplacement of the volcanic rocks of the Paraná-Etendeka Large Igneous Province (PELIP) – Serra Geral Formation, peaked at 134 Ma (Turner et al., 1994; Stewart et al., 1996; de Janasi et al., 2011; Florisbal et al., 2014), covering most of the previous sedimentary successions of the Paraná Basin and possibly portions of the DFB.

Contemporaneous to the upper supersequences of the Paraná Basin, the opening of the South Atlantic Ocean in the Cretaceous (Nürnberg and Müller, 1991; Chang et al., 1992; Torsvik et al., 2009) led to the formation of several passive margin basins as well as important fracture zones. Eastward of the study area, the mostly offshore Pelotas and Santos Basins developed on top of the Catarinense Shield, accumulating a thick sedimentary pile in the continental margin (Bueno et al., 2007; Milani et al., 2007b). The Pelotas Basin is mainly characterized as a volcanic margin, with thick wedges of seaward-dipping reflectors extending from the Florianópolis region to Argentina (Bueno et al., 2007; Bueno, 2021). On the other hand, the Santos Basin lacks the expressive volcanism of the Pelotas Basin, although it has records of a thick evaporite layer that is absent in the Pelotas Basin (Talwani and Abreu, 2000; Milani et al., 2007b; Moreira et al., 2007). Significant fracture zones also developed simultaneously with the opening of the South Atlantic Ocean, such as the Florianópolis Fracture Zone (São Paulo ridge), in *E*-W direction (Gamboa and Rabinowitz, 1981), which is expressed as a volcanic high that extends from the oceanic crust towards

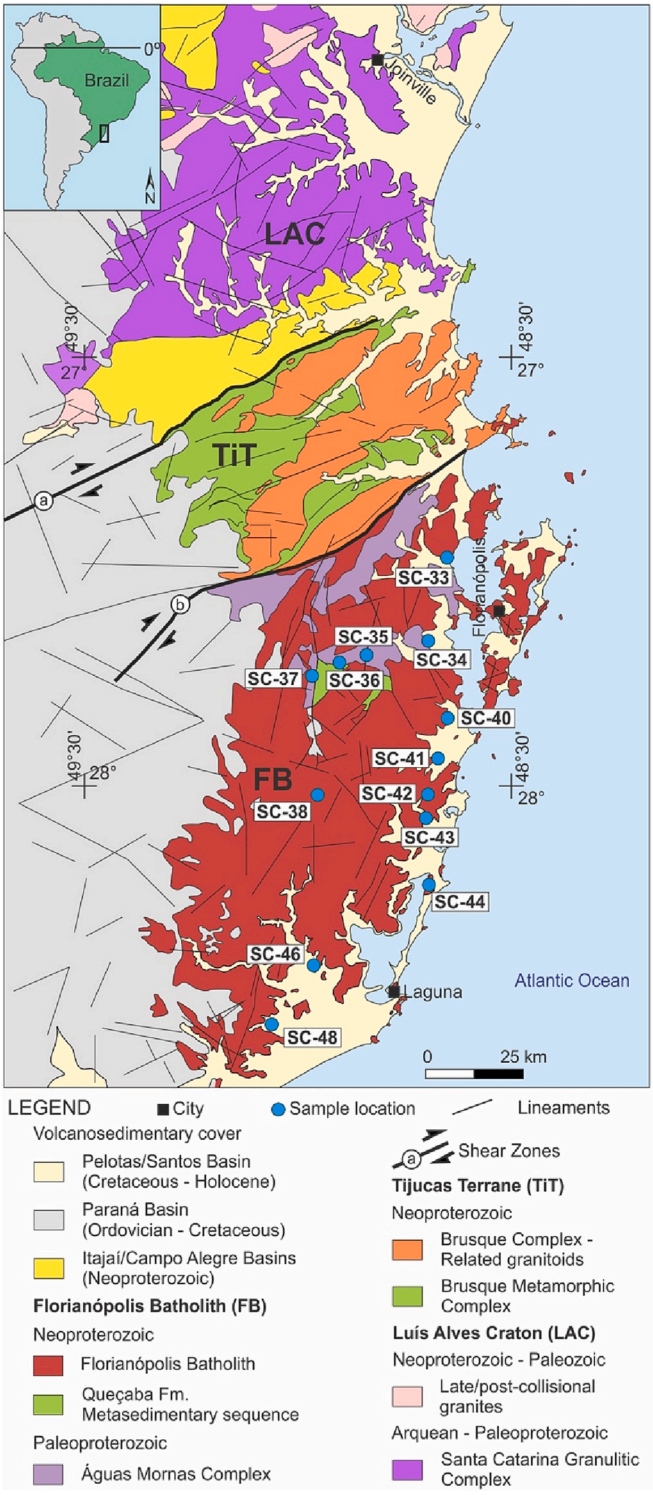

Fig. 2. The study area of this work comprises the Catarinense Shield and its main terranes. Sampling sites are shown in the figure and were restricted to the Florianópolis Batholith. Shear Zones: a: Itajaí-Perimbó Shear Zone; b: Major-Gercino Shear Zone. After CPRM (2014).

the platform near Florianópolis (Mohriak et al., 2008b; Mohriak and Fainstein, 2012).

3. Sampling and analytical methods

3.1. Sampling approach

For this study, basement samples were collected from 13 outcrops over southern Brazil in the eastern portion of the Florianópolis Batholith in the Catarinense Shield, of Neoproterozoic age. We targeted lithologies rich in apatites (granites and gneisses) and we avoided locations that were already sampled in other studies. The collection of samples also followed two main transects of N-S and W-E direction to evaluate spatial variations in thermochronological results. Sampling along vertical profiles was not possible, because the study area presents low topographic prominence, where the average elevation is below 500 m and the highest peak is nearly 1.200 m above sea level. The details of the lithology, geographical location, elevation, shortest distance to the coast, and analytical methods performed in each sample are found in Table 1. Standard crushing, sieving, magnetic, heavy liquids, and hand-picking methods were performed to obtain the apatite crystal separates for both apatite fission track and apatite (U—Th)/He analyzes.

3.2. Low-temperature thermochronometry

To investigate the Phanerozoic thermotectonic evolution of the Catarinense Shield and then compare it with the evolution of the entire DFB, this study applied a joint use of two low-temperature thermochronometers: apatite fission-track (AFT) and apatite (U—Th)/He (AHe). These radio-isotopic systems have different temperatures in which the radiogenic isotopes or features retained within the crystal lattice. Such retention occurs in the temperature interval of ca. 120 and 40 °C, which is compatible with the shallower portions of the crust. At temperatures higher than the specified range of each thermochronometer, radiogenic products are lost through diffusion/annealing and the apparent age tends to zero.

3.2.1. Apatite Fission-Track

The apatite fission-track method is based on the spontaneous fission of ^{238}U that generates linear defects in the apatite crystal lattice. The accumulation of these features is analyzed in terms of their areal density and length, providing the age and the thermal history that a sample has experienced (Price and Walker, 1963; Fleischer et al., 1975). At temperatures higher than 120 °C apatites rapidly anneal, whereas they are stable in temperatures below 60 °C in geological time scales. When apatites are in the temperature interval ranging from 120 to 60 °C, their fission tracks shrink, specifying a temperature window called the apatite fission-track partial annealing zone (AFTPAZ - Gleadow and Duddy, 1981; Gleadow et al., 1986; Green et al., 1986). Temperature is the main factor controlling annealing, even though the apatite chemical composition and the radiation damage are also fundamental factors playing a role in track-fading (Carlson et al., 1999; Barbarand et al., 2003a; Tagami and O'Sullivan, 2005). The areal density of natural, spontaneous tracks relative to the areal density of induced tracks formed after neutron irradiation in a nuclear reactor will provide the apparent age for this sample (Tagami and O'Sullivan, 2005; Reiners et al., 2017). The track-length frequency obtained from horizontal confined fission tracks (Laslett et al., 1982), on the other hand, will provide information regarding the sample's thermal history (Barbarand et al., 2003b; Gleadow et al., 1986).

In this study, the external detector method (EDM; Hurford, 1990) was used. For that, aliquots of apatite crystals from 13 samples were mounted in epoxy resin, polished to expose internal surfaces, and chemically etched with 5.5 M HNO_3 at 21 °C for 20 s to reveal the spontaneous fission tracks (Carlson et al., 1999). Low-uranium muscovite sheets were closely attached to the apatite crystals, U-doped glass dosimeters (CN5), and Durango age standards. Then, the mounts were placed in irradiation cans forming a stack and they were sent to be neutron-irradiated at the IEA-R1, IPEN-CNEN Reactor, São Paulo, Brazil. Next, the muscovite sheets were etched in 48% HF at 20 °C for 18 min to reveal the induced fission tracks (Fleischer and Price, 1964). Samples were dated at LabModel, a thermochronology facility in the Universidade Federal do Rio Grande do Sul. Leica CTR 6000 microscope paired with Leica Application Suite (LAS) software, at 1000 x (dry) magnification, were used to conduct track-count and track-length measurements. AFT ages were calculated based on measurements of at least 20 grains whenever possible, although some samples did not attain that. Calibration of those ages was made according to the ζ-calibration method (Hurford and Green, 1983; Hurford, 1990) and reported as central ages (Galbraith and Laslett, 1993). Chi-squared test to evaluate the AFT ages homogeneity was carried (Galbraith, 1981; Galbraith and Green, 1990) using the RadialPlotter, version 9.4 (Vermeesch, 2009) and fission-track age errors are reported at the 1σ confidence level. With the purpose to analyze the thermal history, we aimed at measuring the length and the c-axis angles of 100 horizontal confined fission tracks in each sample, although most samples failed this criterion. Projection of horizontal confined tracks on the c-axis was also applied since the annealing rates are affected by the orientation of fission tracks relative to this axis (Donelick et al., 1999; Ketcham et al., 2007). The arithmetic mean of about 100 fission-track etch pit diameters (Dpar; e.g. Donelick et al., 2005) were measured as a proxy for apatite composition, which is also a contributing factor to the annealing of the fission tracks.

Table 1
Details from samples analyzed in this study. Coordinates were acquired in UTM zone 22 J, datum WGS84; Dist. Coast: The distance to the Atlantic Ocean; m.a.s.l.: meters above sea level; AFT: Apatite Fission Track dating; AHe: Apatite (U—Th)/He dating.

Sample	Lithology	Easting	Northing	Elevation (m)	Dist. Coast (km)	Method
SC-33	Granitoid	732,808	6,958,339	12	0.07	AFT, AHe
SC-34	Granitoid	727,765	6,937,434	11	3.8	AFT, AHe
SC-35	Granitoid	713,930	6,933,863	150	17.9	AFT, AHe
SC-36	Granitoid	706,461	6,931,782	175	25.7	AFT, AHe
SC-37	Granitoid	700,942	6,929,205	162	31.7	AFT, AHe
SC-38	Granitoid	701,100	6,898,422	236	31.8	AFT, AHe
SC-40	Granitoid	732,504	6,917,226	3	3.5	AFT, AHe
SC-41	Granitoid	713,930	6,933,863	5	4.6	AFT
SC-42	Granitoid	726,544	6,898,593	63	6.5	AFT
SC-43	Granitoid	725,429	6,889,783	10	6.8	AFT, AHe
SC-44	Granitoid	725,542	6,873,041	17	2.6	AFT, AHe
SC-46	Granitoid	699,198	6,851,964	13	19.8	AFT
SC-48	Granitoid	690,289	6,839,148	5	14.6	AFT

3.2.2. Apatite (U—Th)/He

The fundamentals of the (U—Th)/He dating rely on the radioactive decay of the ^{238}U, ^{235}U, ^{232}Th, and ^{147}Sm isotopes producing α nuclei (^{4}He), which are retained within the apatite lattice (Reiners et al., 2017). At high temperatures, the apatite crystal loses the radiogenic particle by thermally activated volume diffusion, consequently resulting in an age of zero. On the other hand, at lower temperatures, ^{4}He starts to accumulate, which is defined at ca. 70 °C for the apatite (U—Th)/He thermochronometer. Concurrent production and loss of ^{4}He occurs in the temperature window of 70 to 40 °C, defining the apatite (U—Th)/He partial retention zone (AHePRZ - Wolf et al., 1996, 1998; Stockli et al., 2000; Farley, 2002). Below 40 °C, full retention of ^{4} He occurs. The apatite (U—Th)/He age and the limits of the AHePRZ may be affected by

many factors, such as crystal size (e.g., Reiners and Farley, 2001; Brown et al., 2013), effective uranium concentration – eU (e.g., Flowers et al., 2009; Reiners et al., 2017), parent nuclide zonation (Farley, 2000; Reiners et al., 2017), radiation damage (Shuster et al., 2006; Flowers et al., 2009), high U and Th content in the neighboring crystals (Spiegel et al., 2009; Murray et al., 2014), presence of micro-inclusions rich in U and Th (Fitzgerald et al., 2006), and cooling rates (Ault and Flowers, 2012; Reiners et al., 2017). Samples experiencing monotonic cooling and long residence within the AHePRZ may enhance the effects of the aforementioned factors, sometimes resulting in dispersed AHe ages (Ault and Flowers, 2012; Green and Duddy, 2018).

For the apatite (U—Th)/He technique, four to seven single crystals of six samples were analyzed at the University of Texas at Austin, in the UTChron – (U—Th)/He and U—Pb Geo-Thermochronometry Laboratory. A Nikon SMZ-U/100 stereomicroscope coupled with Nikon cameras was used to select the apatite crystals considering their size, morphology, and absence of visible inclusions and coating. Samples had their dimensions measured for alpha-eject correction (Ft; Farley et al., 1996) and crystals were photographed. Selected crystals were 94.86 to 302.57 μm long and 49.26 to 142.78 μm wide, in most cases having two terminations. The chosen aliquots were added in Pt tubes, followed by degassing under heating conditions imposed by the Nd-YAG laser. A quadrupole mass spectrometer then measured and quantified the extracted gas. Subsequently, the crystals were reclaimed and dissolved in 65% HNO_3 for isotopic determination (U, Th, and Sm) in an Element2 HR-ICP-MS.

3.2.3. Thermal history inversion

In this study, the software QTQt, version 5.7.2 K, was used for inverse modeling (Gallagher et al., 2009; Gallagher, 2012) that employs the Bayesian transdimensional Markov Chain Monte Carlo (MCMC) approach to data inversion. Dpar measurements and c-axis projection of horizontal confined fission tracks (Ketcham et al., 2007) were used to model AFT data, whereas the radiation damage accumulation and annealing model (RDAAM; Flowers et al., 2009) was applied to model AHe data. A single time-temperature constraint representing the present-day surface temperature was set at 20 ± 10 °C. The prior for temperature was set at 70 ± 70 °C. The prior for time ($t_o \pm t_o$) was set as the oldest AFT age or raw AHe age of each sample. The maximum $\partial T/\partial t$ was set at 30 °C/m.y.

Trial models containing only AFT data were performed at first because this method is more reliable and provides a more accurate description of the thermal history when compared to AHe technique, as suggested by Green and Duddy (2018). Then, AHe data was incorporated into these models. Appropriate values for the MCMC algorithm were defined after initial runs of 30,000 iterations. These values were then applied for runs of at least 200,000 random paths.

3.2.4. Previous thermochronology studies and data integration

This study follows the work of Krob et al. (2019) and Machado et al. (2021a, 2021b) that used interpolated maps of temperature through time, integrating both data sets into a single study, coupled with new AFT and AHe data. Apatite fission track, apatite and zircon (U—Th)/He data associated with AFT data from both the northern and southern Dom Feliciano Belt and surrounding cratons as well associated thermal histories were compiled from de Borba et al. (2002, 2003), Jelinek et al. (2003), Gomes (2011), Kollenz (2015), de Oliveira et al. (2016), Gomes and Almeida (2019), Krob et al. (2019), and Machado et al. (2019, 2020). These studies provided the basement thermal information for 128 different locations across the DFB and Rio de la Plata and Luís Alves cratons ranging from 360 to 30 Ma (Supplementary Table 1). The compilation excluded AFT/AHe data collected from borehole samples and that did not have thermal models available. The T-t plots available in the literature list were not remodeled, but had their modeled temperatures compiled at specific time intervals. Most of the thermal histories reconstructed rely only on AFT data (e.g., although some others integrated AFT with zircon fission track, zircon (U—Th)/He, and apatite (U—Th)/He thermochronometers (e.g. de Oliveira et al., 2016; Hueck et al., 2018a, 2018b; Machado et al., 2021a, 2021b). One study used numerical modeling combining low-temperature thermochronometers with K/Ar, $^{40}Ar/^{39}Ar$, U—Pb, Sm—Nd, and Rb—Sr geochronological data for reconstructing the entire thermal history of the samples (Krob et al., 2019), which also incorporated a Paleozoic constraint acknowledging the sedimentary deposition of the Paraná Basin sequences, with temperatures similar to the present-day conditions.

From each thermal model available, the temperature at 12 specific times was obtained from the mean path. With these data for each point, interpolation maps were generated using the Inverse Distance Weighted (IDW) technique, from ArcToolbox, in the software ArcGIS 10.3. The main purpose of such interpolation maps is to have a broad view of the thermal evolution of southern Brazil and Uruguay as well as pinpoint any distinct thermal prints that may distinguish terranes, fault zones, or regions.

4. Results

4.1. Apatite fission-track

We present new AFT data results of 13 samples collected in the Florianópolis Batholith, northern DFB, summarized in Table 2. All AFT ages passed the χ^2 test ($P(\chi^2) > 0.05$) and the single grain ages showed no dispersion, indicating that the central ages correlate to a single population. AFT central ages of this study are displayed in Fig. 3 along with AFT and AHe ages available in the literature. The new ages vary from 126.6 ± 24.1 to 60.3 ± 6.03 Ma, which are mostly Mesozoic (Lower to Upper Cretaceous) with the majority corresponding to the Upper Cretaceous Epoch. Sample SC-36 is the exception in this data set, since its AFT age is the youngest and the only one of the Paleocene Epoch. It was possible to acquire track-length and c-axis angle information from only 10 samples. Three samples lack information regarding AFT length/angle data and one sample did not yield sufficient lengths for a reliable representation of length distribution. Mean horizontal confined fission-track lengths (MTL) data are displayed in Table 2 and Fig. 4a. Overall, MTL is short to medium-sized (9.08 to 12.44 μm), showing unimodal distribution, and the standard deviation is narrow (Table 2 and Fig. 4b). MTL versus Standard Deviation shows a broad negative correlation between these parameters (Fig. 4c). Skewness is variable amongst samples: most of the data set is moderately negative, comprising five samples with values ranging between −0.94 and −0.55). Four samples are symmetrical, and their values span from −0.48 to 0.38, and one sample is moderately positive (value of 0.98). Dpar values range from 1.33 to 1.54 μm.

The trends of AFT ages versus elevation (Fig. 5a) and the shortest distance to the coastline (Fig. 5b) are essentially diffuse, suggesting that these parameters exert little influence on AFT ages of this data set.

Apatite ages calculated using a zeta of 320.24 ± 6.84 for CN5 glass on Brazil reactor.

4.2. Apatite (U—Th)/He

Table 3 presents the results of Apatite (U—Th)/He data. A sum of 34 apatite crystals was dated from six different locations. From this data set, four outliers were detected, were discarded from inversion and discussion (data in underscore italic on Table 3). Corrected AHe ages (F_t; Farley et al., 1996) are essentially Mesozoic (90%), spanning from 153.0 ± 9.2 to 62.5 ± 3.7 Ma. The standard deviation of AHe ages spans from 4.57 to 26.16 Ma and uncertainties (2σ) are within 2.5 and 11.1%. Apatite single grain eU concentration varies from 4.5 to 96 μg/g, lacking a correlation between this parameter and the corrected AHe ages (Fig. 5a). Equivalent Spherical Radius (ESR) ranges between 26.4 and 72.4 μm and its correlation with AHe ages is absent (Fig. 6b). The elevation and the distance to the coastline versus AHe ages produces a

Table 2
New Apatite Fission Track data from the Catarinense Shield, in the northern Dom Feliciano Belt, southern Brazil. Underscore italic data are outliers, which were discarded from inversion.

Sample	N	ρs (Ns)	ρi (Ni)	ρd (Nd)	P (χ2)	U	Centr. Age ± 1σ	n	MTL	Std. Dev.	P. MTL	P.Std. Dev.	Dpar	Skewness
	#	(x10^5)	(x10^5)	(x10^5)	(%)	(μg/g)	(Ma)	#	(μm)	(μm)	(μm)	(μm)	(μm)	
SC-33	16	7.68 (53)	7.83 (54)	8.14 (16,276)	1	12.2	126.6 ± 24.1	*	*	*	*	*	*	*
SC-34	20	9.55 (85)	12.58 (112)	8.14 (16,276)	1	20.1	98.1 ± 14.7	16	11.59	1.89	13.39	1.44	1.41	−0.58
SC-35	20	17.75 (142)	15.88 (127)	6.06 (6055)	0.99	33.3	107.5 ± 12.9	100	12.44	1.68	13.78	1.35	1.46	−0.94
SC-36	20	16.94 (144)	36.47 (310)	8.14 (16,276)	1	56.9	60.3 ± 6.0	100	12.24	1.66	13.75	1.13	1.37	−0.27
SC-37	20	10.69 (124)	19.14 (222)	8.14 (16,276)	0.98	29.9	72.4 ± 8.0	57	11.92	1.77	13.47	1.31	1.40	−0.55
SC-38	20	9.80 (98)	15.30 (153)	8.14 (16,276)	1	23.9	82.9 ± 10.8	76	11.93	1.88	13.49	1.41	1.54	−0.1
SC-40	20	7.08 (68)	8.85 (85)	8.14 (16,276)	0.98	13.8	103.4 ± 16.5	*	*	*	*	*	*	*
SC-41	20	13.00 (104)	13.38 (107)	6.06 (6055)	1	28.1	93.6 ± 13.1	100	12.06	1.93	13.55	1.39	1.49	−0.63
SC-42	16	15.96 (217)	27.21 (370)	8.14 (16,276)	0.96	42.5	76.0 ± 6.8	16	11.81	1.56	13.48	1.3	1.33	−0.48
SC-43	20	7.15 (118)	8.30 (137)	8.14 (16,276)	0.96	13.0	111.3 ± 14.5	*	*	*	*	*	*	*
SC-44	20	15.50 (124)	22.75 (182)	8.14 (16,276)	0.89	35.5	88.2 ± 10.6	43	10.87	1.71	12.77	1.24	1.40	0.38
SC-46	20	13.75 (110)	17.75 (142)	8.14 (16,276)	1	27.7	100.2 ± 13.0	43	11.90	2.25	13.59	1.47	1.50	−0.81
SC-48	20	12.95 (101)	17.31 (135)	8.14 (16,276)	0.87	27.0	96.8 ± 12.6	6	9.08	2.90	11.83	2.12	1.37	0.98

N: number of apatite crystals analyzed to determine track densities; ρs: measured spontaneous track density; Ns: number of spontaneous tracks counted; ρi: measured induced track density; Ni: number of induced tracks counted; ρd: track density measured in external detector adjacent to glass dosimeter during irradiation; Nd: number of tracks counted in determining ρd; P (χ2): chi-squared probability; n: number of confined track lengths measured; * no horizontal confined track length measured; Centr. Age: Central Age; Std. Dev.: Standard Deviation; P.MTL: Projected mean track length; P.Std. Dev.: Standard Deviation of Projected mean track length.

sparse correlation between these parameters (Fig. 6c and d).

4.3. Thermal history modeling

Fig. 7 presents the thermal histories modeled for 10 samples and the remaining samples were not modeled because they did not yield enough track length data. Models containing AFT and AHe data constrain both higher and lower portions of the time-temperature chart whereas some models for which there are less track-length data display thermal histories that contain large 95% credible envelopes. All samples display good agreement for AHe single grain ages, plotting in the 1:1 line or near it, though there are some exceptions. On the other hand, AFT observed ages are younger than the predicted ones, mostly falling off the 1:1 line.

The thermal histories provided in Fig. 7 are poorly constrained before 150 ± 20 Ma, a period for which they display low relative probability. We analyzed both the weighted mean path and the relative probability indicated in the charts of Fig. 7. Based on that, the samples can be divided into three groups that present somewhat similar trajectories: the first group is comprised of samples SC-35, SC-36, SC-38, SC-44, and SC-46, the second group is comprised of samples SC-34 and SC-41, and the third group comprises samples SC-37 and SC-42. Sample SC-48 was not considered in any group because it failed to generate a constrained thermal history due to the lack of horizontal confined tracks.

In general, Group 1 starts to cool between 120 and 110 Ma, from temperatures in the range of 95 to 70 °C, with the samples cooling to present-day surface conditions, followed by some degree of reheating for most of them (Fig. 7). Samples SC-44 and SC-46 recorded accelerated cooling from 120 to 100 Ma and 110 to 90 Ma, respectively. Sample SC-44 recorded slow reheating of nearly 20 °C to ca. 40 °C from 100 until 15 Ma, followed by final cooling to a surface temperature of 20 °C. Sample SC-46, on the contrary, remained at surface conditions since 90 Ma. Sample SC-36 recorded fast cooling as well, although lasting longer, from 120 to 80 Ma, until reaching 30 °C. Then, a reheating of 20 °C to ca. 50 °C until 15 Ma was recorded, followed by final cooling to the present-day surface temperature. Sample SC-35 displays protracted continuous cooling from 120 Ma until the present day. Sample SC-38 cooled until 50 °C at 90 Ma and reheated until 75 °C at 70 Ma, although it displays a low relative probability. Next, this sample cooled to the present-day surface temperature at 50 Ma, remaining in this condition since then.

Belonging to Group 2, sample SC-34 displayed accelerated cooling from 80 to 60 Ma at temperatures of 65 to 15 °C, remaining in this condition until the present day (Fig. 7). Sample SC-41 started to slowly cool from 150 Ma until 110 Ma from the temperature of 85 to 60 °C, reheated until 70 °C at 80 Ma also lacking high relative probability, and rapidly cooled from 70 to 25 °C from 80 to 60 Ma, remaining in similar conditions to the present-day surface temperature since then.

Lastly, Group 3, composed of samples SC-37 and SC-42, started to cool at 100 until 50 Ma, from nearly 80 °C to ca. 50 °C. The temperature remained stable for nearly 30 Ma for sample SC-37, followed by reheating of 10 °C and then cooling to the surface. Sample SC-42 remained at 50 °C until 10 Ma and then cooled to present-day surface temperature (Fig. 7), although the inverse model lacks high probability, but presents a similar cooling trend with SC-35.

4.4. Basement temperatures assessment

The assessment of basement temperatures of the DFB and surrounding cratons since the beginning of the Carboniferous is presented in Fig. 8. These maps were generated using the Inverse Distance Weighted interpolation technique after reuniting thermal information of 128 locations.

The top row maps evidence the basement temperatures during the Carboniferous (Fig. 8). As it is shown, the temperatures of the DFB and

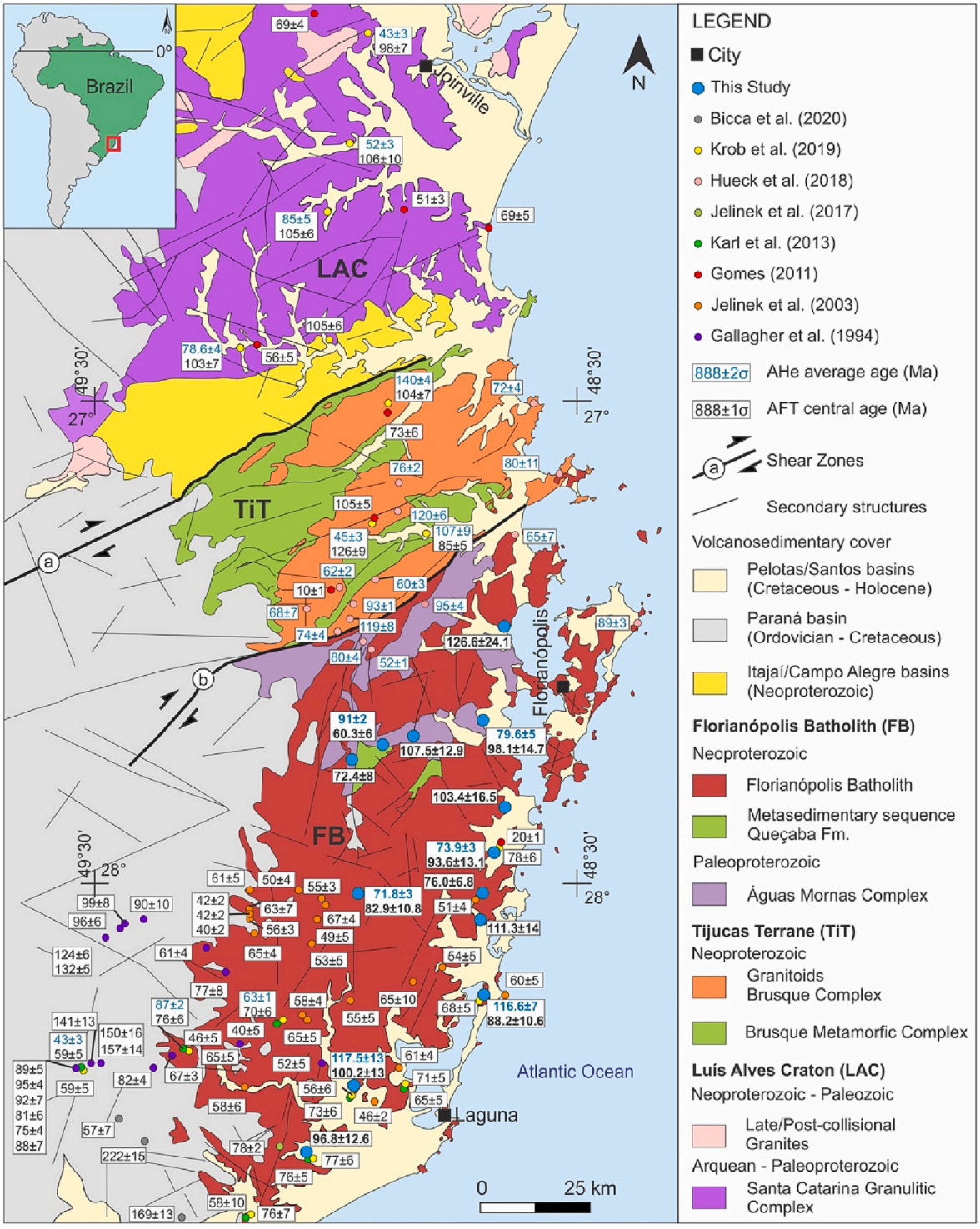

Fig. 3. Compilation of Apatite Fission Track and Apatite (U—Th)/He ages available for the Catarinense Shield and surrounding sediments. Results presented in this study are shown in bold. After CPRM (2014) and (Jelinek et al., 2021).

adjacent cratons at the beginning of the Carboniferous Period were below 180 °C. The Taquarembó Terrane and the western portion of the RDLP were cooler than the southern DFB to the east. However, the Catarinense Shield to the south of Florianópolis city in the northern DFB was at temperatures below 60 °C. At 300 Ma, the rocks from this region were at their coolest temperature, residing on the surface or in extremely shallow portions of the crust, which is the result of the restriction imposed in the models of (Krob et al., 2019), forcing the models to run in low temperatures.

During the Permian, at 270 Ma, most of the RDLP, the southern end and central portions of the DFB, and the Taquarembó Terrane were at temperatures below 90 °C. Surrounding these cooler portions, restrained regions of temperatures no higher than 120 °C remained, as it is seen in the top end of the southern DFB near Porto Alegre city and close to the border between Uruguay and the Rio Grande do Sul state, both regions composing the Pelotas Batholith. In the northern DFB, a heating trend from north to south evidences that the Catarinense Shield had an increase in temperature to nearly 90 °C. This pattern is maintained

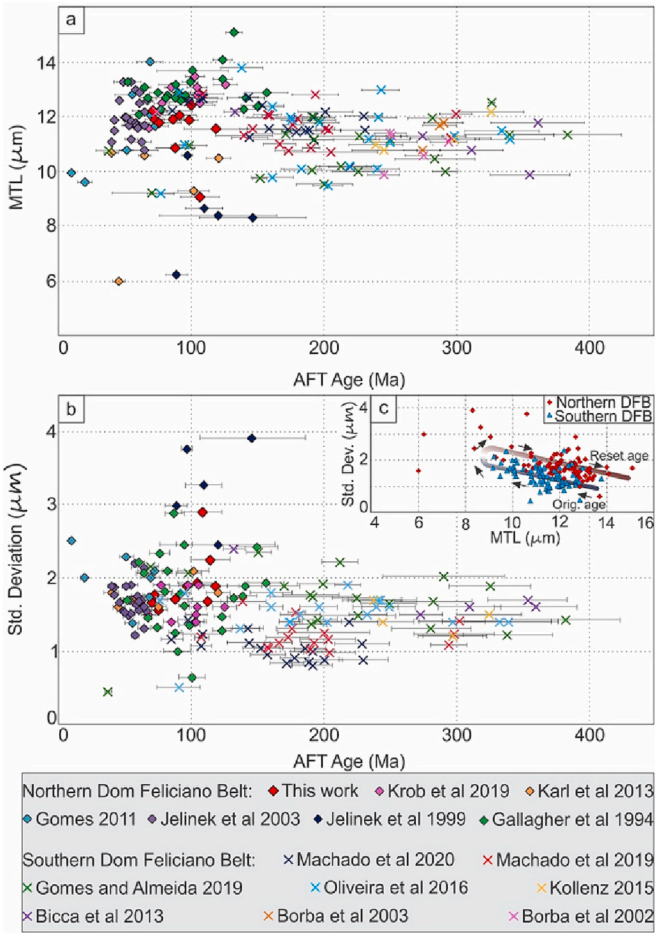

Fig. 4. Compiled Apatite Fission Track (AFT) ages of this study and from the literature plotted against a) Mean Track Length (MTL) and b) Standard Deviation (Std. Dev). c) Mean Track Lengths versus Standard Deviation. The AFT ages of the Uruguayan and Sul-Rio-Grandense shield are somewhat similar and grouped into the "Southern Dom Feliciano Belt" data set. AFT ages for the northern and southern Dom Feliciano Belt are shown as diamonds and X shapes, respectively. Error bars (1σ) are shown in the charts. Abbreviation is Orig. age: original age.

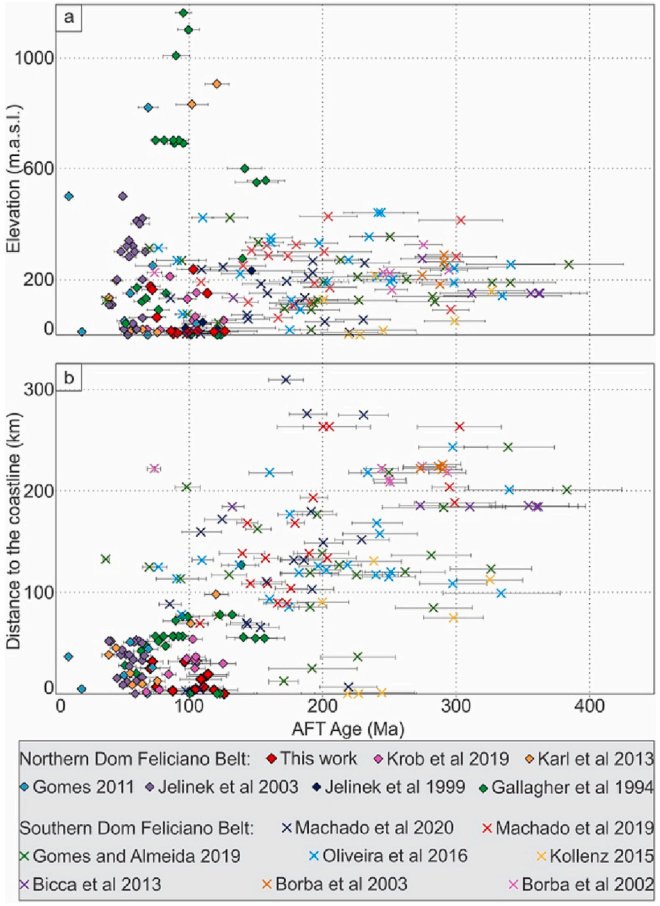

Fig. 5. Compiled central Apatite Fission Track ages (AFT) of this study and available in the literature plotted against a) Elevation; b) Distance to the coastline. Error bars (1σ) are shown in the charts. Abbreviation is: m.a.s.l.: meters above sea level.

throughout the Triassic and Jurassic, reaching its higher temperature, 150 °C, by 210 to 180 Ma (Fig. 8).

The southern DFB and the neighboring RDLP, on the other hand, remained in a cooling trend. At 180 Ma, temperatures in the region were cooler than 90 °C, and in some locations even cooler than 30 °C, such as the western portion of the RDLP and in the Pelotas Batholith in Uruguay. Before rifting at 150 Ma, most of the SRGS and Uruguayan Shields were at 60 °C or less. Contrasting to this pattern, the northern DFB were at temperatures ranging from 150 to 60 °C, at 150 Ma (Fig. 8).

From the opening of the South Atlantic Ocean, at 120 Ma, until 30 Ma, a distinct temperature pattern remains between the northern DFB and LAC in comparison with the southern DFB and RDLP. In the south, temperatures were no higher than 90 °C at 120 Ma, cooling to nearly 30 °C by the end of Paleogene. In the north, temperatures varied from 120 to 60° at 120 Ma, rapidly cooling to ~60–30 °C at 30 Ma. It is noteworthy that to the south of Florianópolis city the temperature remained a little higher than 60 °C until 30 Ma, contrasting to its neighboring craton and the whole SRGS and Uruguayan Shields (Fig. 8).

5. Discussion

5.1. Distribution of apatite fission track ages in the Northern and Southern Dom Feliciano Belt

In this work, we contributed 13 new AFT ages for the Catarinense Shield, located in the northern DFB (Table 2). The AFT ages presented here as well as a compilation of AFT ages of studies performed along the DFB and adjacent cratons are plotted against MTL (Fig. 4a) and standard deviation (Fig. 4b). The younger AFT ages, essentially from samples of the northern DFB, are mostly associated with long to intermediate tracks that are usually generated after rapid cooling or experienced a strong degree of annealing. The samples from this area present AFT ages younger than 150 Ma, suggesting that a reheating event raised temperatures high enough to reset AFT and AHe thermochronometers. The lack of well-defined thermal histories before 150 Ma is due to the complete thermal resetting of the AFT and AHe data used for thermal modeling. The thermal resetting in the northern DFB was caused by the emplacement of volcanic rocks belonging to the PELIP and associated feeding dyke swarms (Florisbal et al., 2014, 2018; Hueck et al., 2018a), causing a reheating event, raising the temperatures across the northern DFB. For the southern DFB, the fission track lengths are mostly short to intermediate, reflecting long residence at higher temperatures under some degree of annealing in the AFTPAZ. There is no apparent correlation between the standard deviation and AFT ages of samples analyzed. However, the samples of the northern DFB and LAC display values between 1 and 2.5 μm, whereas the southern DFB and RDLP

Table 3
Summary of Apatite (U—Th)/He ages and parameters; The abbreviations reported in table are: eU: effective uranium, calculated as eUμg/g = [Uμg/g + (0.235*Thμg/g) + 0.00463*Smμg/g)]; Ft: Correction Factor after (Farley et al., 1996); ESR: Equivalent Spherical Radius; Corr.: Corrected; SD: Standard Deviation; Aver.: Average. Italic and underscored data point to outlier samples (outliers) and discarded from inversion.

Sample	Grain #	He (nmol/g)	U (μg/g)	Th (μg/g)	Sm (μg/g)	eU (μg/g)	Mass (μg)	ESR (μm)	Raw Age (Ma)	± 2σ (Ma)	Ft #	Corr. Age (Ma)	± 2σ (Ma)	Aver. Corr. (Ma)	± 2σ (Ma)	SD (Ma)
SC-34	1	4.7	9.2	27.7	513.7	18.2	2.9	47.4	43.0	2.58	0.67	64.0	3.8	79.64	4.82	12.75
SC-34	2	3.1	5.4	17.1	371.4	11.2	4.1	47.7	46.1	2.77	0.67	68.4	4.1			
SC-34	3	1.9	2.9	7.6	191.3	5.6	2.6	45.0	56.4	3.38	0.66	85.7	5.1			
SC-34	4	2.7	5.1	15.0	321.4	10.1	1.9	41.0	43.9	2.63	0.63	70.0	4.2			
SC-34	6	4.5	6.8	17.9	384.8	12.8	3.1	50.7	58.4	3.51	0.69	84.3	5.1			
SC-34	7	1.8	1.9	7.8	154.1	4.5	1.8	43.2	64.4	3.86	0.64	100.3	6.0			
SC-34	8	4.1	6.4	20.3	397.2	13.0	1.7	40.2	52.6	3.16	0.62	84.8	5.1			
SC-36	*1*	*27.1*	*84.8*	*20.0*	*423.8*	*91.5*	*4.5*	*56.1*	*53.8*	*3.23*	*0.74*	*72.9*	*4.4*	91.05	2.29	4.57
SC-36	2	13.4	29.4	4.6	226.8	31.6	9.0	72.4	76.1	4.57	0.80	95.7	5.7			
SC-36	*3*	*27.9*	*55.7*	*11.0*	*337.8*	*59.9*	*2.9*	*47.6*	*84.2*	*5.05*	*0.70*	*120.8*	*7.2*			
SC-36	4	26.6	74.1	19.4	403.9	80.6	2.9	49.8	60.0	3.60	0.71	84.9	5.1			
SC-36	5	23.7	59.1	8.3	312.5	62.6	5.4	59.8	68.6	4.12	0.76	90.8	5.4			
SC-36	6	32.6	86.2	32.2	473.1	96.0	2.2	43.1	61.6	3.70	0.66	92.7	5.6			
SC-38	1	3.7	8.1	19.6	260.7	13.9	1.0	33.8	45.7	2.74	0.56	81.2	4.9	71.81	3.27	7.30
SC-38	3	8.4	16.1	47.1	480.9	29.3	2.4	45.7	50.1	3.00	0.66	75.6	4.5			
SC-38	4	5.4	10.0	34.6	452.4	20.2	5.0	59.5	45.8	2.75	0.73	62.5	3.7			
SC-38	5	4.0	7.3	26.0	313.6	14.9	3.4	50.4	46.2	2.77	0.69	67.0	4.0			
SC-38	6	11.6	21.2	67.0	670.7	40.0	3.3	51.3	50.6	3.03	0.69	72.8	4.4			
SC-38	*7*	*12.4*	*15.8*	*57.4*	*517.9*	*31.6*	*3.4*	*52.1*	*68.2*	*4.09*	*0.70*	*97.7*	*5.9*			
SC-41	1	3.7	6.6	14.1	259.1	11.1	3.8	50.2	56.4	3.38	0.69	81.6	4.9	73.97	2.82	6.29
SC-41	*2*	*7.2*	*10.9*	*27.0*	*427.9*	*19.3*	*2.5*	*41.8*	*64.0*	*3.84*	*0.64*	*100.7*	*6.0*			
SC-41	3	9.9	20.8	54.0	401.4	35.2	2.3	45.4	49.7	2.98	0.66	75.3	4.5			
SC-41	4	5.7	15.0	38.7	396.3	25.9	1.0	32.3	38.5	2.31	0.54	70.7	4.2			
SC-41	5	6.5	11.4	32.9	438.3	21.1	3.9	48.9	52.6	3.16	0.68	77.1	4.6			
SC-41	6	6.3	14.3	42.9	368.1	26.0	2.6	43.9	42.3	2.54	0.65	65.2	3.9			
SC-44	2	7.2	13.3	45.5	229.0	25.0	0.6	28.7	51.5	3.09	0.49	104.2	6.3	116.65	6.71	15.00
SC-44	5	10.5	14.1	51.5	359.5	27.8	1.6	41.8	66.1	3.97	0.63	104.5	6.3			
SC-44	6	25.4	31.6	123.0	548.8	62.6	0.7	30.2	71.8	4.31	0.51	139.9	8.4			
SC-44	7	20.1	23.5	91.9	453.0	46.9	2.5	48.3	75.7	4.54	0.68	112.0	6.7			
SC-44	8	7.1	10.2	24.9	186.7	16.9	1.3	38.1	74.1	4.45	0.60	122.6	7.4			
SC-46	1	14.1	16.7	54.5	381.7	31.2	3.2	49.0	79.5	4.77	0.68	116.7	7.0	117.55	13.08	26.16
SC-46	2	8.2	7.4	20.6	273.8	13.5	2.8	48.3	103.8	6.23	0.68	153.0	9.2			
SC-46	5	12.0	23.9	103.9	667.9	51.2	0.5	26.4	41.2	2.47	0.46	90.3	5.4			
SC-46	7	10.0	16.1	44.7	345.8	28.1	1.0	34.3	62.5	3.75	0.57	110.3	6.6			

exhibit values between 1 and 2 μm. According to Green (1986), as the annealing proceeds until total resetting, the older tracks fade, resulting in larger mean tracks and the reduction of the standard deviation values with a consequent AFT age reduction, generating distinct patterns in the standard deviation versus AFT age plot. Additionally, the plot of MTL versus standard deviation (Fig. 4c) shows that samples from the southern DFB and RDLP are clustered in the lower portion of the chart (Green, 1986), which may represent the "original age" of the AFT thermochronometer for this region. The "original age" in this case represents the age that the apatites would have if they were not disturbed by reheating events, representing original cooling ages. Considering this, the samples from the northern DFB and LAC are, therefore, interpreted as reset AFT ages, which are plotted slightly above the samples from the Southern DFB in Fig. 4c. As said before, the northern DFB AFT ages represent reset ages, i.e., after the original cooling these samples were reheated in varying degrees until they were totally annealed. To corroborate our interpretation, the detrital AFT ages of rocks from the Paraná Basin located to the west to the Catarinense Shield exhibit Carboniferous ages similar to the AFT ages of the southern DFB (Bicca et al., 2020). Thus, we suggest that the Carboniferous ages may represent the timing of exposure of the shield to temperatures cooler than 60 °C following the tectonic assembly of the shield.

The elevation and the shortest distance to the coastline are other criteria used to discuss AFT ages and their distribution. The data set presented here fails to demonstrate a correlation between these parameters with AFT ages, contrasting with the trends usually recognized for this thermochronometer in Brazil in specific studies (e.g. Amaral-Santos et al., 2019; Gallagher et al., 1994; Machado et al., 2019).

5.2. Apatite (U—Th)/He intra and intersample age variations

In this study, we presented 30 new AHe ages from six samples of the Catarinense Shield, in the northern DFB. Apatite (U—Th)/He intra-sample age dispersion is small for most samples (see SD column in Table 3). For all samples the selected apatite crystals were free of inclusions, preventing parentless ^{4}He to be added to the apatite crystal lattice (Lippolt et al., 1994). U and Th-rich minerals that neighbor the apatite crystals are also other possible sources of He implantation. However, this data set does not exhibit any anomalously old AHe age, from which we deduce that these samples are free of He implantation.

Additionally to extraneous ^{4}He, the radiation damage plays a fundamental role as a source of intra- and intersample age variation, since it strongly influences He diffusion, inducing high-eU apatites to retain fractional He and producing old AHe ages. This effect is demonstrated by a positive non-linear correlation between these parameters (Flowers et al., 2009). This data set, however, shows a non-existent correlation between AHe ages and eU concentration (Fig. 6a), suggesting additional sources of noise that control the distribution of AHe ages. A monotonic fast cooling scenario that could explain the lack of correlation above is discarded because the western portion of the Florianópolis Batholith may have been exposed to surface conditions during the Paleozoic when the first units of the Paraná Basin were deposited (Krob et al., 2019), as other parts of the Uruguayan and SRGS may have. Furthermore, this region probably experienced reheating during burial as well as reheating during the emplacement of the PELIP and associated feeding dykes (see 5.3 section) that reset both AHe and AFT thermochronometers, which argue against a monotonic cooling thermal history.

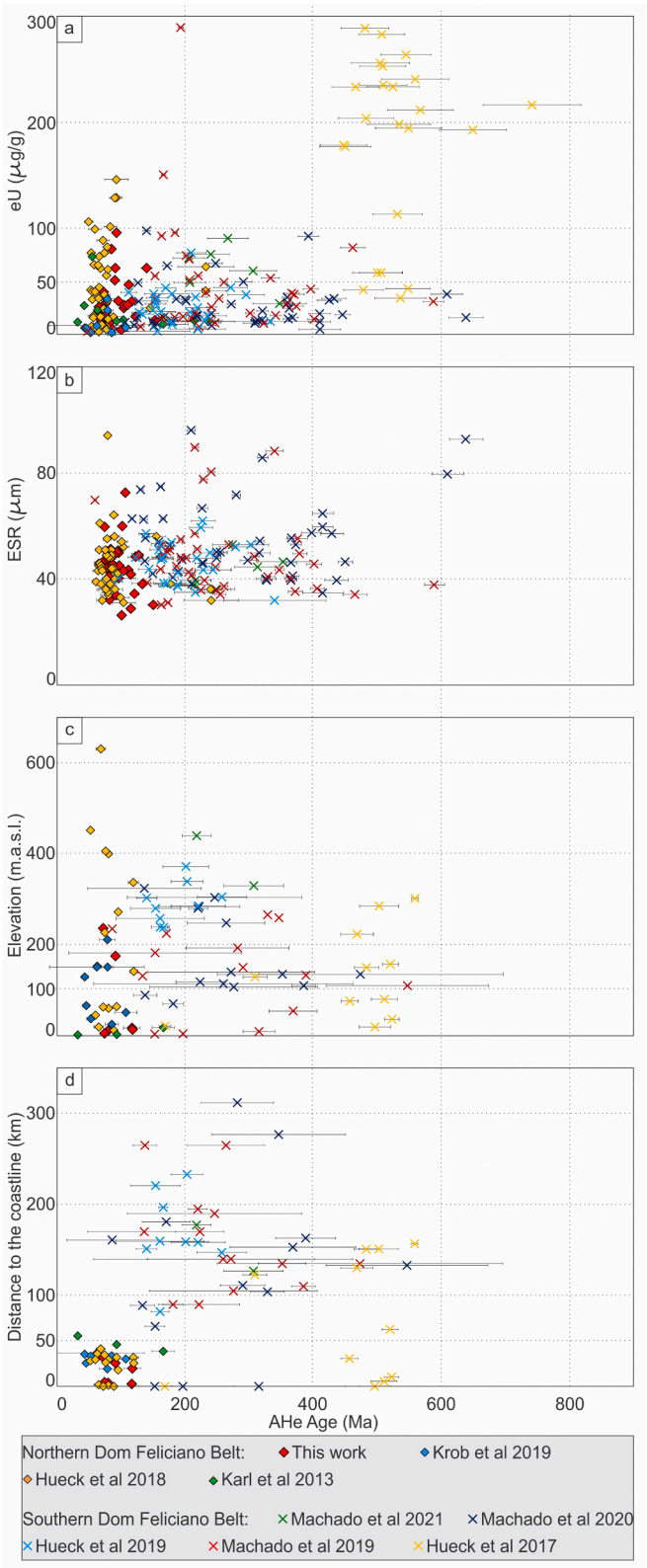

Fig. 6. Apatite (U—Th)/He ages for all crystals analyzed in this study and available in the literature plotted against a) Effective uranium concentration (eU), b) Equivalent Spherical Radius (ESR). Mean Apatite (U—Th)/He ages in each sample of this study and in the literature plotted against c) Elevation and d) Distance to the coastline. Error bars (2σ) are shown for each sample.

The grain size, referred to as ESR in this study, is also a parameter used to asses (U—Th)/He ages dispersion (Brown et al., 2013; Reiners and Farley, 2001). In this new data set, the AHe ages do not display a clear correlation with ESR (Fig. 6b). The lack of correlation can indicate simple rapid cooling in the range of this thermochronometer or over-dispersion (Brown et al., 2013). Indeed, the thermal histories presented here display accelerated Meso-Cenozoic cooling. From a regional perspective, the relationship between the ESR and the AHe ages of samples collected in the northern and southern segments of the DFB and surrounding cratons fails to demonstrate a distinct correlation between these parameters. However, the northern DFB seems to relate to the first approach in which rapid cooling is the engine driving the lack of correlation, while in the southern DFB the driving mechanism is the over-dispersion of ages (e.g., Hueck et al., 2017, 2018a, 2019; Machado et al., 2019, 2020).

The intersample AHe age variation, similar to AFT data, fails to correlate with elevation and the shortest distance to the coastline.

Dispersion amongst samples of this new data set also generated a pattern of inverted AFT and AHe ages, in which some of AHe ages are older than their AFT ones. These inverted ages are not explained by the analyzes performed in this study, nor by a series of works that have the same issues, which can be attributed to problems in understanding He diffusion systematics (Green and Duddy, 2018).

5.3. *Timing and spatial patterns inferred from thermochronology and data interpolation*

The new compilation presented in this study allows us to recognize and discuss regional trends for the studied area.

During the Carboniferous, the temperature of the entire DFB and adjacent cratons was below 180 °C (Fig. 8), with these rocks placed at mid to shallow portions of the upper crust. Exhumation of these rocks during the Paleozoic was affected by the Gondwanic Orogenic Cycle (Milani and Ramos, 1998) through intraplate stress propagation, causing surface uplift and inducing erosion, as proposed for other West Gondwana intraplate environments (e.g., Jelinek et al., 2014; Engelmann de Oliveira et al., 2016; Amaral-Santos et al., 2019; Martins-Ferreira et al., 2020; do Amaral Santos et al., 2022). The Northern DFB and LAC were possibly exhumed by the Carboniferous as well, displaying temperatures compatible with near-surface conditions (Krob et al., 2019). These conditions exposed on our maps may be due to the constraints imposed before samples were modeled in the work of Krob et al. (2019). On the other hand, detrital AFT ages of sedimentary rocks from the Paraná basin range from Carboniferous to Miocene (Bicca et al., 2020), suggesting that older AFT ages may correlate with the northern DFB exhumation during the Carboniferous. AFT thermal modeling of these samples collected from boreholes to the west of Catarinense Shield advocates in favor of a surface to near-surface exposure from the end of the Paleozoic until the end of the Jurassic (Bicca et al., 2020). Detrital ZHe and ZFT ages of sedimentary samples of the Paraná basin (Karl et al., 2013) also suggest provenance ages related to the exhumation of the northern DFB and its partial exposure during the Carboniferous. By the end of this period, two supersequences of the Paraná Basin had already been deposited to the north of the LAC and the Gondwana I supersequence started its deposition during the Permian-Carboniferous, reaching a thickness of nearly 2.5 km (Milani et al., 2007a, 2007b). The units of the latter outcrop to the west and in some places within the Catarinense Shield, suggesting that the shield was, at least, partially covered by the sediments of the Paraná Basin. At that time, the sedimentary overload in the northern DFB reached nearly the thickness of 4 km, heating the basement, indicated by the reset of the AFT and AHe ages in the area, which is demonstrated by the maps shown in Fig. 8, from 300 to 210 Ma, and also advocated by Krob et al. (2019).

During the Triassic to the end of the Jurassic, both the Uruguayan and SRGS shields experienced gradual cooling, recording temperatures between 90 and 30 °C (Fig. 8). Such trend suggests that before rifting,

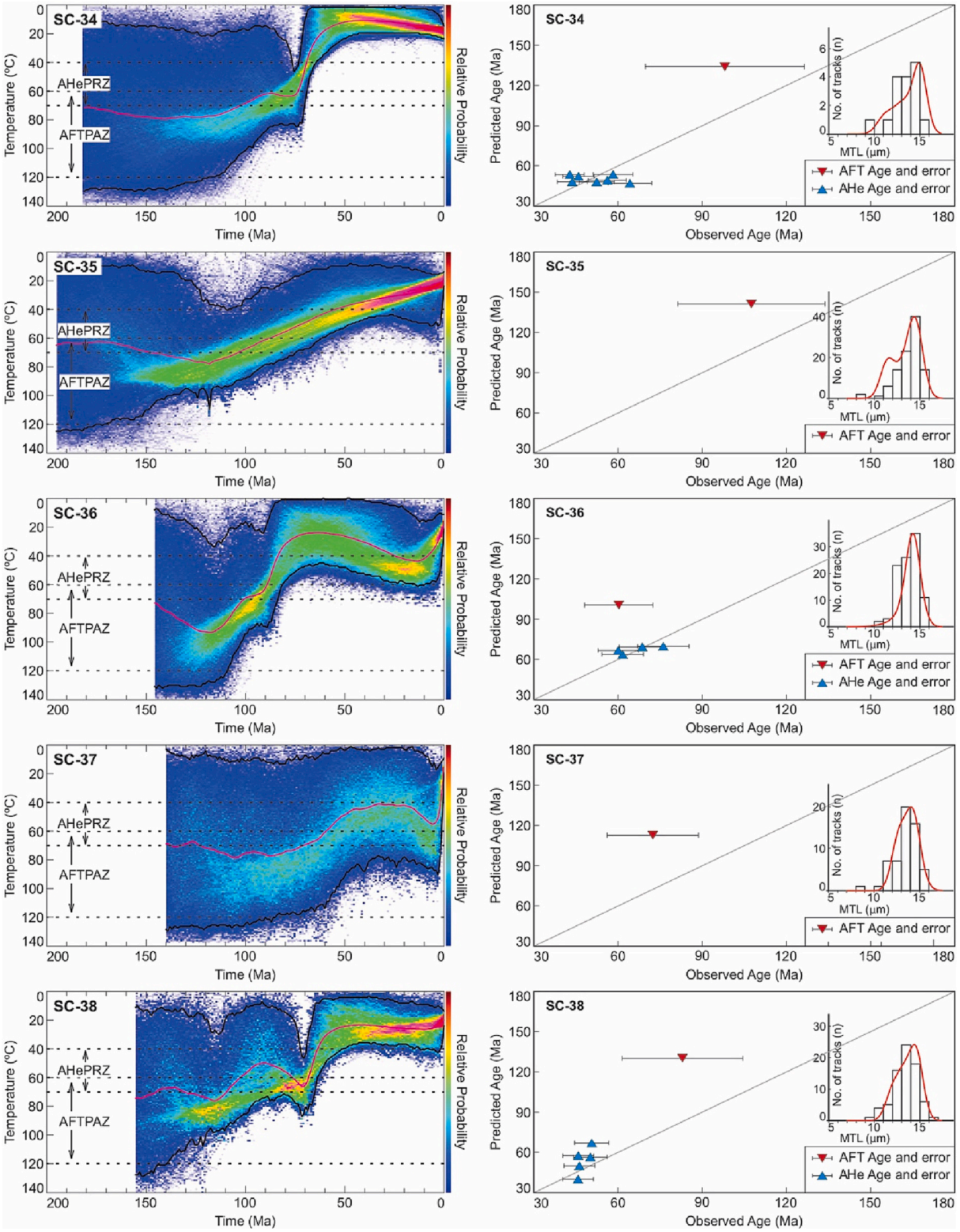

Fig. 7. Inverse modeling results generated in QTQt (Gallagher, 2012) for samples SC-34, SC-35, SC-36, SC-37, SC-38, SC-41, SC-42, SC-44, SC-46 and SC-48. The 95% credible interval defines the expected model (black curves). The weighted mean path is represented by the magenta curve. The range of the AFTPAZ and AHePRZ is defined by the dashed lines. The relative probability scale increases from blue to red. On the right of the thermal histories are shown observed versus predicted ages charts. Upside-down red triangles indicate AFT ages whereas AHe single-crystal ages are displayed in upside-pointing blue triangles. The Mean Track Length (MTL) distribution of AFT data is represented as bars, with the red line indicating track lengths modeled. (For interpretation of the references to colour in this figure legend, the reader is referred to the web version of this article.)

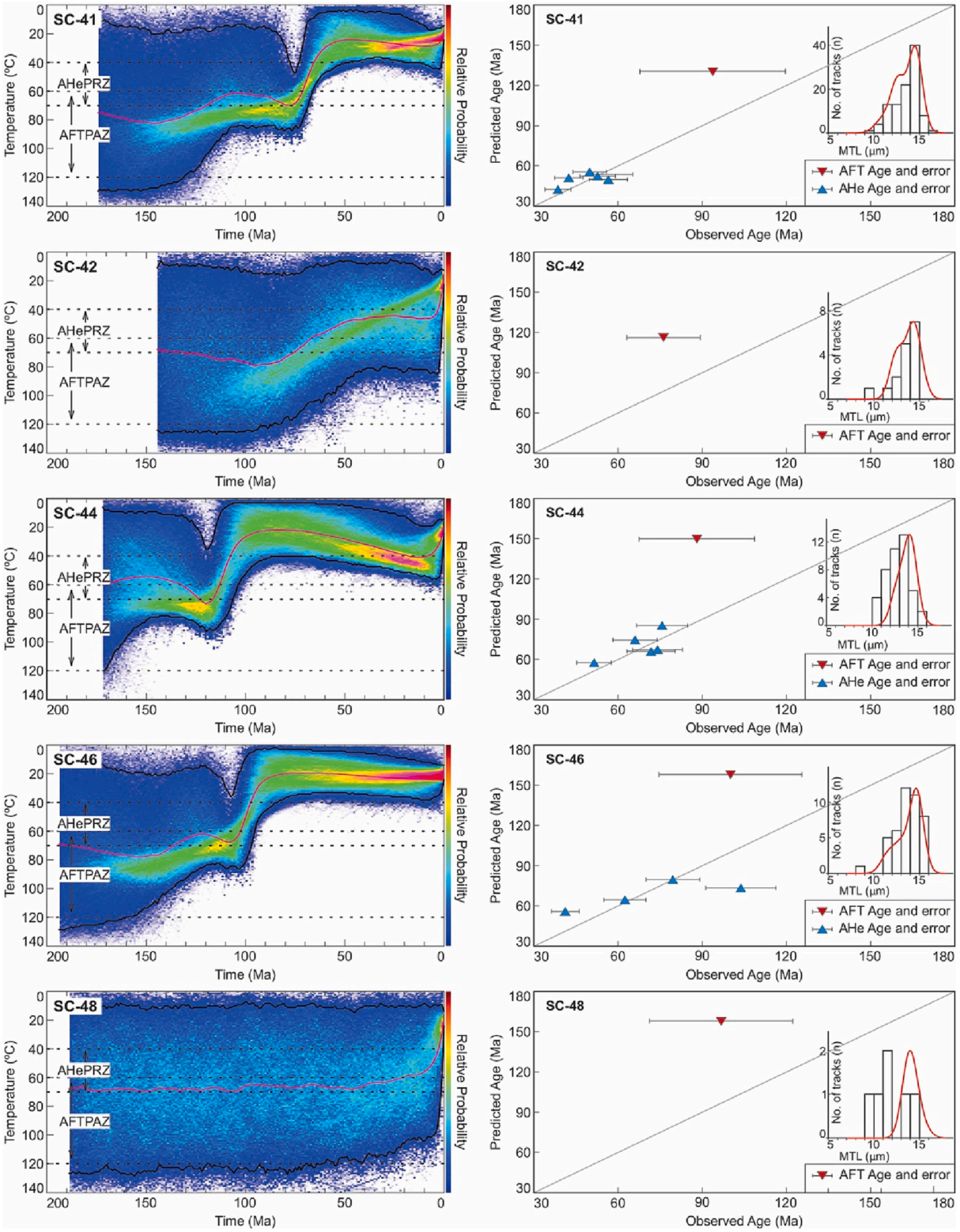

Fig. 7. (*continued*).

these shields were at low temperatures, in similar conditions to near-surface environments. Machado et al. (2021a, 2021b) suggested that the RDLP and the southern DFB likely cooled down between 110 and 60 °C in the Mesozoic. For the same area, Hueck et al. (2017, 2019) proposed a hypothesis of near-surface exposure much earlier, by the Silurian, with possible reheating after that leading to samples remaining in temperatures higher than 60 °C until the Triassic. Favoring the assumption of near-surface conditions by the end of the Paleozoic to the Mesozoic advocated by Jelinek et al. (2021) and Machado et al. (2021a, 2021b), conglomerates and sandstones of the Sanga do Cabral Formation of Triassic age (Lavina, 1988) were deposited within the SRGS, suggesting that it was already exposed to near-surface conditions (low temperatures) during the Triassic. Considering that thermochronologic data is quite widespread, it is also important to emphasize that the

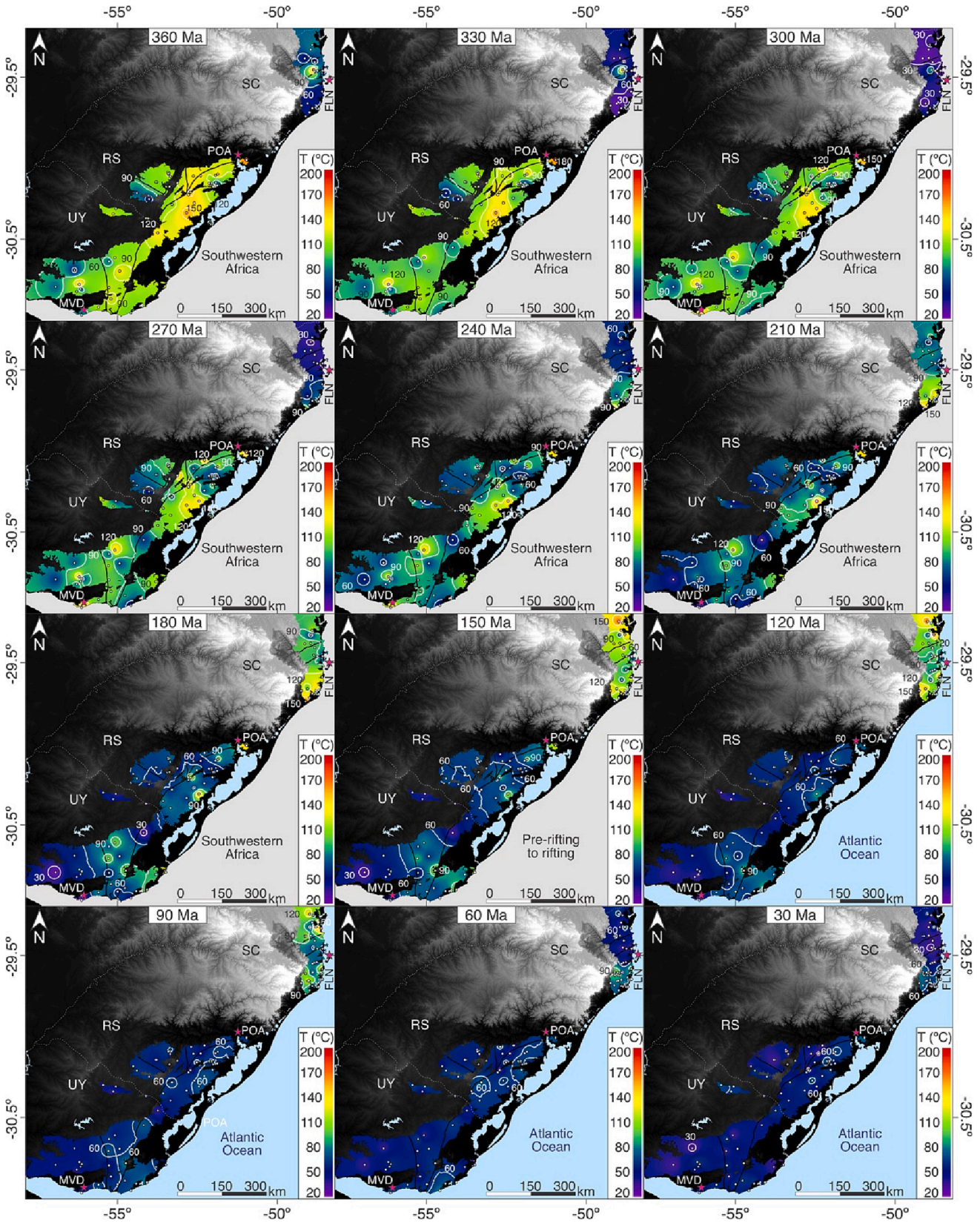

Fig. 8. Basement temperatures across the Dom Feliciano Belt and surrounding cratons from 360 to 30 Ma assessed by the Inverse Distance Weighted (IDW) interpolation technique. The time-temperature points were obtained from inverse models from this work and de Borba et al. (2002, 2003), Jelinek et al. (2003), Gomes (2011), Kollenz (2015), de Oliveira et al. (2016) Gomes and Almeida (2019), Krob et al. (2019), Machado et al. (2019, 2020) Red stars indicate the country or state capital city. Abbreviations are: SC: Santa Catarina State; RS: Rio Grande do Sul State; UY: Uruguay; FLN: Florianópolis; POA: Porto Alegre; MVD: Montevideo. (For interpretation of the references to colour in this figure legend, the reader is referred to the web version of this article.)

thermal history recovered for the area is broad and that papers may have differences in what they highlight. In the Lower Cretaceous, the SRGS was cut by feeding dykes of the PELIP, even though only localized reheating was recorded by samples in the eastern Pelotas Batholith (Hueck et al., 2019; Machado et al., 2019). Moreover, Paleozoic AFT ages of the southern DFB and RDLP (Fig. 8) suggest minor to absent resetting caused the emplacement of the PELIP volcanic rocks, as suggested by Hueck et al. (2019).

On the other hand, the Catarinense Shield was at higher temperatures by the end of the Jurassic, with some locations recording 150 °C (Fig. 8). The heating increment lasted until the Lower Cretaceous, with the emplacement of the PELIP at approximately 134 Ma (Turner et al., 1994; Stewart et al., 1996; de Janasi et al., 2011). This extensive volcanic event induced reheating in the northern DFB and LAC, causing total annealing of the AFT and AHe thermochronometers (e. g., This work, Gallagher et al., 1994; Jelinek et al., 2003; Karl et al., 2013; Krob et al., 2019, 2020) and the partial to total resetting of ZHe and ZFT thermochronometers (Karl et al., 2013; Hueck et al., 2018a, 2018b; Krob et al., 2019). This is demonstrated by AFT and AHe ages similar or younger than the volcanic emplacement, thermal histories based on AFT data that do not span to times older than nearly 150 Ma, overly dispersed ZHe ages (Hueck et al., 2018a), and some Cretaceous ZFT and ZHe ages (Karl et al., 2013). Besides, the feeding dykes of the PELIP located in the Catarinense Shield (Florisbal et al., 2014, 2018; Wildner et al., 2014), in N*E*-SW direction, may also be responsible for elevating the geothermal gradient in the area, which would reinforce the annealing caused by the emplacement of the PELIP, as advocated by some authors (e.g., Hueck et al., 2018a, 2018b; Krob et al., 2019) and acknowledged in this study. Another possible source of heating during the Upper Jurassic to Lower Cretaceous is the alkaline-carbonatitic intrusions in the northern DFB (Anitápolis intrusion – ca. 132 Ma; Sonoki and Garda, 1988; Gibson et al., 2006; Ferreira et al., 2022) and to the north of the LAC, in the Ponta Grossa Arch region (Amaral et al., 1997). Some of these intrusions are found on or close to NW-SE lineaments, which acted as a conduit for the lavas of the PELIP in a long and wide fissure zone (Riccomini et al., 2005). For all this, before rifting several sources of heating in the northern DFB and LAC were present, reshaping the geothermal gradient of the upper crust and resetting low-temperature thermochronometers, which completely opposes the processes operating in the southern DFB and RDLP.

The extrusions of the volcanic rocks of the PELIP were coeval to the opening of the southernmost South Atlantic basin in the Upper Jurassic to the Lower Cretaceous (Rabinowitz and Labrecque, 1979; Torsvik et al., 2009; Moulin et al., 2010; Heine et al., 2013) and preceded seafloor spreading located to the east of the Catarinense Shield, which occurred approximately between 120 and 115 Ma (Heine et al., 2013). The thermal histories presented in this study suggest that some samples experienced the onset of accelerated cooling following breakup and seafloor spreading (Fig. 7). A few AFT ages are contemporaneous with these tectonic processes (Table 2), suggesting that rifting may have induced exhumation of the Catarinense Shield. In addition to this, the temperature of the basement at 120 Ma ranged from 150 °C to nearly 60 °C, implying that some of the sources of heating mentioned earlier were still active. Conversely, the southern DFB and RDLP were in cooler temperatures during breakup as observed in the 120 Ma-map of Fig. 8.

Finally, during the Upper Cretaceous (90 Ma) to the Eocene (30 Ma) the drift phase of the South America plate was on course, recording the formation of sedimentary basins of the eastern Brazilian continental margin (e.g., Milani et al., 2007b; Mohriak et al., 2008b; Machado et al., 2021a, 2021b; Ferreira et al., 2022). Moreover, the emplacement of alkaline-carbonatitic intrusions in the SRGS, in the Catarinense Shield, and throughout the Mantiqueira Province were registered (Ferreira et al., 2022), implying sources of heat that Riccomini et al. (2005) attributed to long-lived mantle upwelling. Many AFT and AHe ages from this study and in the literature and some thermal models display fast cooling coeval to these events. Cogné et al. (2011), in their study in the Ribeira Belt to the north of the study area, related the Upper Cretaceous to the Paleogene cooling to a thermally weakened crust subject to plate-wide compression possibly associated with post-rifting magmatism or earlier mantle plume activity and structural inheritance. Important to notice, however, is that the mechanisms cited above were not only associated with cooling but also with post-rift uplift of the passive margin. However, in the northern DFB a prominent escarpment is somewhat absent while this geomorphic feature is completely absent in the southern DFB. We, therefore, acknowledge this argument and we suggest that the prolonged higher temperature of the northern DFB and LAC in comparison with the southern DFB and RDLP (Fig. 8) is due to the closer proximity of the northern DFB to the Florianópolis Fracture Zone (Mohriak et al., 2010), of *E*-W direction. This fracture zone represents leaky faults related to the emplacement of volcanic plugs during the Upper Cretaceous to the Eocene (Mohriak et al., 2010) and, hence, a conduit for heating transport. Furthermore, a prominent NW-SE lineament named Cruzeiro do Sul is associated with the Florianópolis Fracture Zone and related to a major plate reorganization in the Paleogene to Neogene (Mohriak, 2004; Mohriak et al., 2010). At that time, several igneous plugs were emplaced both onshore and offshore in the Santos Basin, to the north of the study area, and, hence, could be a source of heat supply.

6. Conclusion

In this work, we contributed with 13 new AFT ages and 30 new apatite (U—Th)/He ages of samples collected in the Catarinense Shield, in the northern Dom Feliciano Belt. Both AFT and corrected AHe ages are essentially Mesozoic and MTL are short to medium associated with reset AFT ages.

Additionally, we assessed the basement temperatures for 128 locations across the entire DFB and adjacent cratons – Rio de La Plata and Luís Alves – since the Carboniferous, presented in 12 maps. Since the Paleozoic, the northern and southern DFB experienced contrasting thermal histories. The southern DFB was possibly exhumed to near-surface temperatures by the end of the Permian, being subject to minor reheating only in a few places until the present day. Conversely, the northern DFB was probably exposed to near-surface conditions in the Carboniferous and partially buried by the sediments of the Paraná basin megasequences, interpreted from data compiled from the literature that used constraints that forced models to run in low temperatures and from detrital AFT, ZFT and ZHe ages to the west of the study area. From the Mesozoic to the Eocene, the region was strongly reheated by the (1) emplacement of the volcanic rocks of the Paraná-Etendeka Large Igneous Province; (2) presence of a feeding dyke system of the same LIP, and (3) intrusion of alkaline-carbonatitic rocks mostly associated with the Florianópolis Fracture Zone, of E-W direction. Therefore, we suggest that the northern DFB and Luís Alves Craton region recorded a series of mutual events responsible for keeping the temperature high enough to induce the annealing of the fission tracks and the diffusion of α particles in apatite, causing age dispersion and resetting partial to totally these low-temperature thermochronometers, completely contrasting to the Meso-Cenozoic thermal history of the southern Dom Feliciano Belt and Rio de La Plata craton.

Several issues remain open and should be answered in future works; for example, (1) the extent of annealing conditions for AFT and AHe thermochronometers to the north of the locations sampled in this study; (2) the trends of AFT age versus elevation/distance to the coastline for samples located to the continent interior and at higher elevations; (3) the role of E-W and NW-SE fracture zones affecting the thermochronological record, such as the Florianópolis Fracture Zone exemplified in this study.

CRediT authorship contribution statement

Edgar do Amaral Santos: Conceptualization, Methodology,

Validation, Formal analysis, Investigation, Writing – original draft, Visualization. **Andréa Ritter Jelinek:** Conceptualization, Methodology, Formal analysis, Writing – review & editing, Supervision, Project administration, Funding acquisition. **Daniel Stockli:** Formal analysis, Resources. **Frederico Antônio Genezine:** Formal analysis, Resources.

Declaration of Competing Interest

The authors declare that they have no known competing financial interests or personal relationships that could have appeared to influence the work reported in this paper.

Data availability

Data will be made available on request.

Acknowledgments

E. Amaral-Santos thanks the Ph.D scholarship provided by the Conselho Nacional de Desenvolvimento Científico e Tecnológico – CNPq, for (140775/2019-6). A.R. Jelinek thanks to the Conselho Nacional de Desenvolvimento Científico e Tecnológico - CNPq (Project 309329/2020-5). The authors thank M.M. Bicca for assistance with AFT data. The authors thank the Tectonophysics Editor Dr. Zheng-Xiang Li, the reviewer Dr. Mathias Hueck, and an anonymous reviewer that helped to improve an earlier version of this manuscript.

Appendix A. Supplementary data

Supplementary data to this article can be found online at https://doi.org/10.1016/j.tecto.2023.229841.

References

Amaral, G., Born, H., Hadler, J.C.N., Iunes, P.J., Kawashita, K., Machado, D.L., Oliveira, E.P., Paulo, S.R., Tello, C.A.S., 1997. Fission track analysis of apatites from São Francisco craton and Mesozoic alcaline-carbonatite complexes from central and southeastern Brazil. J. S. Am. Earth Sci. 10, 285–294. https://doi.org/10.1016/s0895-9811(97)00020-5.

Amaral-Santos, E., Jelinek, A.R., Almeida-Abreu, P.A., Genezine, F.A., 2019. Phanerozoic cooling history of Archean/Paleoproterozoic basement in the southern Espinhaço Range, southeastern Brazil, through apatite fission-track analysis. J. S. Am. Earth Sci. 96, 102352 https://doi.org/10.1016/j.jsames.2019.102352.

Ault, A.K., Flowers, R.M., 2012. Is apatite U-Th zonation information necessary for accurate interpretation of apatite (U-Th)/he thermochronometry data? Geochim. Cosmochim. Acta 79, 60–78. https://doi.org/10.1016/j.gca.2011.11.037.

Barbarand, J., Carter, A., Wood, I., Hurford, T., 2003a. Compositional and structural control of fission-track annealing in apatite. Chem. Geol. 198, 107–137. https://doi.org/10.1016/S0009-2541(02)00424-2.

Barbarand, J., Hurford, T., Carter, A., 2003b. Variation in apatite fission-track length measurement: Implications for thermal history modelling. Chem. Geol. 198, 77–106. https://doi.org/10.1016/S0009-2541(02)00423-0.

Basei, M.Â.S., 1985. O Cinturão Dom Feliciano em Santa Catarina. University of São Paulo, p. 213.

Basei, M.A.S., Siga Jr., O., Machiavelli, A., Mancini, F., 1992. Evolução Tectônica Dos Terrenos Entre Os Cinturões Ribeira E Dom Feliciano (Pr-Sc). Rev. Bras. Geociências 22, 216–221. https://doi.org/10.25249/0375-7536.1992216221.

Basei, M.A.S., McReath, I., Siga, O., 1998. The Santa Catarina Granulite complex of Southern Brazil: a Review. Gondwana Res. 1, 383–391. https://doi.org/10.1016/S1342-937X(05)70854-6.

Basei, M.A.S., Frimmel, H.E., Nutman, A.P., Preciozzi, F., 2008. West Gondwana amalgamation based on detrital zircon ages from Neoproterozoic Ribeira and Dom Feliciano belts of South America and comparison with coeval sequences from SW Africa. Geol. Soc. Spec. Publ. 294, 239–256. https://doi.org/10.1144/SP294.13.

Basei, M.A.S., Peel, E., Bettucci, L.S., Preciozzi, F., Nutman, A.P., 2011. The basement of the Punta del Este Terrane (Uruguay): an African Mesoproterozoic fragment at the eastern border of the South American Río de La Plata craton. Int. J. Earth Sci. 100, 289–304. https://doi.org/10.1007/s00531-010-0623-1.

Bicca, M.M., Kalkreuth, W., da Silva, T.F., de Oliveira, C.H.E., Genezini, F.A., 2020. Thermal and depositional history of Early-Permian Rio Bonito Formation of southern Paraná Basin – Brazil. Int. J. Coal Geol. 228, 103554 https://doi.org/10.1016/j.coal.2020.103554.

Brown, R.W., Beucher, R., Roper, S., Persano, C., Stuart, F., Fitzgerald, P., 2013. Natural age dispersion arising from the analysis of broken crystals. Part I: Theoretical basis and implications for the apatite (U-Th)/he thermochronometer. Geochim. Cosmochim. Acta 122, 478–497. https://doi.org/10.1016/j.gca.2013.05.041.

Bueno, G.V., 2021. Bacia de Pelotas em retrospectiva. In: Jelinek, A.R., Sommer, C.A. (Eds.), Contribuições à Geologia Do Rio Grande Do Sul e de Santa Catarina. Compasso Lugar-Cultura, Porto Alegre, pp. 389–402.

Bueno, G.V., Zacharias, A.A., Oreiro, S.G., Cupertino, J.A., Falkenhein, F.U.H., Martins-Neto, M.A., 2007. Bacia de Pelotas. Bol. Geoci. da Petrobras 15, 551–559.

Carlson, W.D., Donelick, R.A., Ketcham, R.A., 1999. Variability of apatite fission-track annealing kinetics: I. Experimental results. Am. Mineral. 84, 1213–1223. https://doi.org/10.2138/am-1999-0901.

Chang, H.K., Kowsmann, R.O., Figueiredo, A.M.F., Bender, A.A., 1992. Tectonics and stratigraphy of the East Brazil Rift system: an overview. Tectonophysics 213, 97–138. https://doi.org/10.1016/0040-1951(92)90253-3.

Cogné, N., Gallagher, K., Cobbold, P.R., 2011. Post-rift reactivation of the onshore margin of Southeast Brazil: evidence from apatite (U–Th)/he and fission-track data. Earth Planet. Sci. Lett. 309, 118–130. https://doi.org/10.1016/j.epsl.2011.06.025.

CPRM, 2008. Mapa Geológico do Estado do Rio Grande do Sul. Porto Alegre, Programa Geologia do Brasil, escala 1:750.000.

CPRM, 2014. Mapa Geológico do estado de Santa Catarina. Porto Alegre, Programa Geologia do Brasil, escala 1:500.000.

de Almeida, F.F.M., Hasui, Y., de Brito Neves, B.B., Fuck, R.A., 1981. Brazilian structural provinces: An introduction. Earth Sci. Rev. 17, 1–29. https://doi.org/10.1016/0012-8252(81)90003-9.

de Borba, A.W., Vignol-Lelarge, M.L.M., Mizusaki, A.M.P., 2002. Uplift and denudation of the Caçapava do Sul granitoids (southern Brazil) during late Paleozoic and Mesozoic: Constraints from apatite fission-tract data. J. S. Am. Earth Sci. 15, 683–692. https://doi.org/10.1016/S0895-9811(02)00086-X.

de Borba, A.W., de Lima, E.F., Vignol-Lelarge, M.L.M., Mizusaki, A.M.P., Sparrenberg, I., de Barros, C.E., 2003. Significance of late Paleozoic fission-track ages in volcanic rocks from the Lavras Do Sul region, southernmost Brazil. Gondwana Res. 6, 79–88. https://doi.org/10.1016/S1342-937X(05)70645-6.

De Brito Neves, B.B., Fuck, R.A., 2013. Neoproterozoic evolution of the basement of the South-American platform. J. S. Am. Earth Sci. 47, 72–89. https://doi.org/10.1016/j.jsames.2013.04.005.

de Janasi, V.A., de Freitas, V.A., Heaman, L.H., 2011. The onset of flood basalt volcanism, Northern Paraná Basin, Brazil: a precise U-Pb baddeleyite/zircon age for a Chapecó-type dacite. Earth Planet. Sci. Lett. 302, 147–153. https://doi.org/10.1016/j.epsl.2010.12.005.

de Oliveira, C.H.E., Jelinek, A.R., Chemale, F., Bernet, M., 2016. Evidence of post-Gondwana breakup in Southern Brazilian Shield: insights from apatite and zircon fission track thermochronology. Tectonophysics 666, 173–187. https://doi.org/10.1016/j.tecto.2015.11.005.

do Amaral Santos, E., Jelinek, A.R., Machado, J.P., Stockli, D., 2022. Thermal history along the Araçuaí Orogen and São Francisco Craton border, eastern Brazilian continental margin, based on low-temperature thermochronologic data. Tectonophysics 825, 229232. https://doi.org/10.1016/j.tecto.2022.229232.

Donelick, R.A., Ketcham, R.A., Carlson, W.D., 1999. Variability of apatite fission-track annealing kinetics: II. Crystallographic orientation effects. Am. Mineral. 84, 1224–1234. https://doi.org/10.2138/am-1999-0902.

Donelick, R.A., O'Sullivan, P.B., Ketcham, R.A., 2005. Apatite fission-track analysis. In: Reiners, P.W., Ehlers, T.A. (Eds.), Reviews in Mineralogy and Geochemistry, pp. 49–94. https://doi.org/10.2138/rmg.2005.58.3.

Engelmann de Oliveira, C.H., Jelinek, A.R., Chemale, F., Cupertino, J.A., 2016. Thermotectonic history of the southeastern Brazilian margin: evidence from apatite fission track data of the offshore Santos Basin and continental basement. Tectonophysics 685, 21–34. https://doi.org/10.1016/j.tecto.2016.07.012.

Farley, K., 2000. Helium diffusion from apatite, General behavior as illustrated by Durango fluorapatite the implied He closure temperature for a grain. J. Geophys. Res. 105, 2903–2914.

Farley, K.A., 2002. (U-Th)/He dating: Techniques, calibrations, and applications. Rev. Mineral. Geochem. 47, 819–844. https://doi.org/10.2138/rmg.2002.47.18.

Farley, K., Wolf, R., Silver, L., 1996. The effects of long alpha-stopping distances on (U-Th)/He ages. Geochim. Cosmochim. Acta 60, 4223–4229. https://doi.org/10.1016/S0016-7037(96)00193-7.

Ferreira, A.C.D., Conceição, R.V., Mizusaki, A.M.P., 2022. Mesozoic to Cenozoic alkaline and tholeiitic magmatism related to West Gondwana break-up and dispersal. Gondwana Res. 106, 15–33. https://doi.org/10.1016/j.gr.2022.01.005.

Fitzgerald, P.G., Baldwin, S.L., Webb, L.E., O'Sullivan, P.B., 2006. Interpretation of (U-Th)/he single grain ages from slowly cooled crustal terranes: a case study from the Transantarctic Mountains of southern Victoria Land. Chem. Geol. 225, 91–120. https://doi.org/10.1016/j.chemgeo.2005.09.001.

Fleischer, R.L., Price, P.B., 1964. Techniques for geological dating of minerals by chemical etching of fission fragment tracks. Geochim. Cosmochim. Acta 28, 1705–1714. https://doi.org/10.1016/0016-7037(64)90017-1.

Fleischer, R.L., Price, P.B., Walker, R.M., 1975. Nuclear Tracks in Solids: Principles and Applications. University of California Press, California.

Florisbal, L.M., Heaman, L.M., de Assis Janasi, V., de Fatima Bitencourt, M., 2014. Tectonic significance of the Florianópolis Dyke Swarm, Paraná-Etendeka Magmatic Province: a reappraisal based on precise U-Pb dating. J. Volcanol. Geotherm. Res. 289, 140–150. https://doi.org/10.1016/j.jvolgeores.2014.11.007.

Florisbal, L.M., Janasi, V.A., Bitencourt, M.F., Nardi, L.V.S., Marteleto, N.S., 2018. Geological, geochemical and isotope diversity of ~ 134 Ma dykes from the Florianópolis Dyke Swarm, Paraná Magmatic Province: Geodynamic controls on petrogenesis. J. Volcanol. Geotherm. Res. 355, 181–203. https://doi.org/10.1016/j.jvolgeores.2017.08.002.

Flowers, R.M., Ketcham, R.A., Shuster, D.L., Farley, K.A., 2009. Apatite (U-Th)/he thermochronometry using a radiation damage accumulation and annealing model.

Geochim. Cosmochim. Acta 73, 2347–2365. https://doi.org/10.1016/j.gca.2009.01.015.
Galbraith, R.F., 1981. On statistical models for fission track counts. J. Int. Assoc. Math. Geol. 13, 471–478. https://doi.org/10.1007/BF01034498.
Galbraith, R.F., Green, P.F., 1990. Estimating the component ages in a finite mixture. Int. J. Radiat. Appl. Instrumentat. 17, 197–206. https://doi.org/10.1016/1359-0189(90)90035-V.
Galbraith, R.F., Laslett, G.M., 1993. Statistical models for mixed fission track ages. Int. J. Radiat. Appl. Instrumentat. 21, 459–470. https://doi.org/10.1016/1359-0189(93)90185-C.
Gallagher, K., 2012. Transdimensional inverse thermal history modeling for quantitative thermochronology. J. Geophys. Res. Solid Earth 117, B02408. https://doi.org/10.1029/2011JB008825.
Gallagher, K., Hawkesworth, C.J., Mantovani, M.S.M., 1994. The denudation history of the onshore continental margin of SE Brazil inferred from apatite fission track data. J. Geophys. Res. 99, 117–145. https://doi.org/10.1029/94jb00661.
Gallagher, K., Charvin, K., Nielsen, S., Sambridge, M., Stephenson, J., 2009. Markov chain Monte Carlo (MCMC) sampling methods to determine optimal models, model resolution and model choice for Earth Science problems. Mar. Pet. Geol. 26, 525–535. https://doi.org/10.1016/j.marpetgeo.2009.01.003.
Gamboa, L.A.P., Rabinowitz, P.D., 1981. The Rio Grande fracture zone in the western South Atlantic and its tectonic implications. Earth Planet. Sci. Lett. 52, 410–418. https://doi.org/10.1016/0012-821X(81)90193-X.
Gaucher, C., Frei, R., Chemale, F., Frei, D., Bossi, J., Martínez, G., Chiglino, L., Cernuschi, F., 2011. Mesoproterozoic evolution of the Río de la Plata Craton in Uruguay: at the heart of Rodinia? Int. J. Earth Sci. 100, 273–288. https://doi.org/10.1007/s00531-010-0562-x.
Gibson, S.A., Thompson, R.N., Day, J.A., 2006. Timescales and mechanisms of plume-lithosphere interactions: 40Ar/39Ar geochronology and geochemistry of alkaline igneous rocks from the Paraná-Etendeka large igneous province. Earth Planet. Sci. Lett. 251, 1–17. https://doi.org/10.1016/j.epsl.2006.08.004.
Gleadow, A.J.W., Duddy, I.R., 1981. A natural long-term track annealing experiment for apatite. Nucl. Tracks 5, 169–174. https://doi.org/10.1016/0191-278X(81)90039-1.
Gleadow, A.J.W., Duddy, I.R., Green, P.F., Hegarty, K.A., 1986. Fission track lengths in the apatite annealing zone and the interpretation of mixed ages. Earth Planet. Sci. Lett. 78, 245–254. https://doi.org/10.1016/0012-821X(86)90065-8.
Gomes, C.H., 2011. História Térmica Das Regiões Sul E Sudeste Da América Do Sul: Implicações Na Compartimentação Geotectônica Do Gondwana. Universidade Federal do Rio Grande do Sul, Cristiane Heredia Gomes.
Gomes, C.H., Almeida, D., 2019. New insights into the Gondwana breakup at the Southern South America by apatite fission-track analyses. Adv. Geosci. 47, 1–15. https://doi.org/10.5194/adgeo-47-1-2019.
Green, P.F., 1986. On the thermo-tectonic evolution of Northern England: evidence from fission track analysis. Geol. Mag. 123, 493–506. https://doi.org/10.1017/S0016756800035081.
Green, P., Duddy, I., 2018. Apatite (U-Th-Sm)/he thermochronology on the wrong side of the tracks. Chem. Geol. 488, 21–33. https://doi.org/10.1016/j.chemgeo.2018.04.028.
Green, P.F., Duddy, I.R., Gleadow, A.J.W., Tingate, P.R., Laslett, G.M., 1986. At an early stage in the development of fission-track dating , Fleischer et al. (1965) showed that of various environmental param- eters which could possibly affect the long term stability of fission tracks , temperature is by far the dominant factor. Chem. Geol. Isot. Geosci. Sect. 59, 237–253. https://doi.org/10.1016/0168-9622(86)90074-6.
Guadagnin, F., Chemale, F., Dussin, I.A., Jelinek, A.R., dos Santos, M.N., Borba, M.L., Justino, D., Bertotti, A.L., Alessandretti, L., 2010. Depositional age and provenance of the Itajaí Basin, Santa Catarina State, Brazil: Implications for SW Gondwana correlation. Precambrian Res. 180, 156–182. https://doi.org/10.1016/j.precamres.2010.04.002.
Hartmann, L.A., 1998. Deepest exposed crust of Brazil - Geochemistry of paleoproterozoic depleted Santa Maria Chico granulites. Gondwana Res. 1, 331–341. https://doi.org/10.1016/S1342-937X(05)70849-2.
Hartmann, L.A., Campal, N., Santos, J.O.S., McNaughton, N.J., Bossi, J., Schipilov, A., Lafon, J.M., 2001. Archean crust in the Rio de la Plata Craton, Uruguay - SHRIMP U-Pb zircon reconnaissance geochronology. J. S. Am. Earth Sci. 14, 557–570. https://doi.org/10.1016/S0895-9811(01)00055-4.
Hasui, Y., 2010. A grande colisão pré-cambriana do sudeste brasileiro e a estruturação regional. Geociências 29 (2), 141–169.
Heine, C., Zoethout, J., Müller, R.D., 2013. Kinematics of the South Atlantic rift. Solid Earth 4, 215–253. https://doi.org/10.5194/se-4-215-2013.
Hueck, M., Oriolo, S., Dunkl, I., Wemmer, K., Oyhantçabal, P., Schanofski, M., Basei, M.Â.S., Siegesmund, S., 2017. Phanerozoic low-temperature evolution of the Uruguayan Shield along the South American passive margin. J. Geol. Soc. Lond. 174, 609–626. https://doi.org/10.1144/jgs2016-101.
Hueck, M., Dunkl, I., Heller, B., Stipp Basei, M.A., Siegesmund, S., 2018a. (U-Th)/he Thermochronology and Zircon Radiation damage in the South American Passive margin: thermal Overprint of the Paraná LIP? Tectonics 37, 4068–4085. https://doi.org/10.1029/2018TC005041.
Hueck, M., Oyhantçabal, P., Philipp, R.P., Basei, M.A.S., Siegesmund, S., 2018b. The Dom Feliciano Belt in Southern Brazil and Uruguay. In: Siegesmund, S., Basei, M.Â.S., Oyhantçabal, P., Oriolo, S. (Eds.), Geology of Southwest Gondwana. Springer, Cham, pp. 267–302. https://doi.org/10.1007/978-3-319-68920-3_11.
Hueck, M., Dunkl, I., Oriolo, S., Wemmer, K., Basei, M.A.S., Siegesmund, S., 2019. Comparing contiguous high- and low-elevation continental margins: New (U-Th)/He constraints from South Brazil and an integration of the thermochronological record of the southeastern passive margin of South America. Tectonophysics 770, 228222. https://doi.org/10.1016/j.tecto.2019.228222.
Hurford, A.J., 1990. Standardization of fission track dating calibration: recommendation by the Fission Track Working Group of the I.U.G.S. subcommission on geochronology. Chem. Geol. Isot. Geosci. Sect. 80, 171–178. https://doi.org/10.1016/0168-9622(90)90025-8.
Hurford, A.J., Green, P.F., 1983. The zeta age calibration of fission-track dating. Chem. Geol. 41, 285–317. https://doi.org/10.1016/S0009-2541(83)80026-6.
Jelinek, A.R., Bastos Neto, A.C., Poupeau, G., 2003. Análise Por Traços De Fissão Em Apatitas Do Distrito Fluorítico De Santa Catarina: Relações Entre Hidrotermalismo E Evolução Da Margem Continental. Rev. Bras. Geociências 33, 289–298. https://doi.org/10.25249/0375-7536.2003333289298.
Jelinek, A.R., Chemale, F., van der Beek, P.A., Guadagnin, F., Cupertino, J.A., Viana, A., 2014. Denudation history and landscape evolution of the northern East-Brazilian continental margin from apatite fission-track thermochronology. J. S. Am. Earth Sci. 54, 158–181. https://doi.org/10.1016/j.jsames.2014.06.001.
Jelinek, A.R., Machado, J.P.S.L., do Santos, E., 2021. Evolução termocronológica do Cinturão Dom Feliciano: implicações na geodinâmica da margem continental sul do Brasil. In: Jelinek, A.R., Sommer, C.A. (Eds.), Contribuições à Geologia Do Rio Grande Do Sul e de Santa Catarina. Compasso Lugar-Cultura, Porto Alegre, pp. 185–202.
Karl, M., Glasmacher, U.A., Kollenz, S., Franco-Magalhaes, A.O.B., Stockli, D.F., Hackspacher, P.C., 2013. Evolution of the South Atlantic passive continental margin in southern Brazil derived from zircon and apatite (U-Th-Sm)/he and fission-track data. Tectonophysics 604, 224–244. https://doi.org/10.1016/j.tecto.2013.06.017.
Ketcham, R.A., Carter, A., Donelick, R.A., Barbarand, J., Hurford, A.J., 2007. Improved modeling of fission-track annealing in apatite. Am. Mineral. 92, 799–810. https://doi.org/10.2138/am.2007.2281.
Kollenz, S., 2015. Long-Term Landscape Evolution, Cooling and Exhumation History of the South American Passive Continental Margin in NE Argentina & SW Uruguay. Ruprecht-Karls-Universität.
Krob, F.C., Glasmacher, U.A., Karl, M., Perner, M., Hackspacher, P.C., Stockli, D.F., 2019. Multi-chronometer thermochronological modelling of the late Neoproterozoic to recent t-T-evolution of the SE coastal region of Brazil. J. S. Am. Earth Sci. 92, 77–94. https://doi.org/10.1016/j.jsames.2019.02.012.
Krob, F.C., Glasmacher, U.A., Bunge, H.-P., Friedrich, A.M., Hackspacher, P.C., 2020. Application of stratigraphic frameworks and thermochronological data on the Mesozoic SW Gondwana intraplate environment to retrieve the Paraná-Etendeka plume movement. Gondwana Res. 84, 81–110. https://doi.org/10.1016/j.gr.2020.02.010.
Laslett, G.M., Kendall, W.S., Gleadow, A.J.W., Duddy, I.R., 1982. Bias in measurement of fission-track length distributions. Nucl. Tracks Radiat. Meas. 6, 79–85. https://doi.org/10.1016/0735-245X(82)90031-X.
Lavina, E.L., 1988. The Passa Dois Group. In: Internation Gondwana Symposium, 7. 1988. São Paulo. Field Excursion Guide Book. Instituto de Geociências, São Paulo, pp. 24–30.
Lippolt, H.J., Leitz, M., Wernicke, R.S., Hagedorn, B., 1994. (Uranium + thorium)/helium dating of apatite: experience with samples from different geochemical environments. Chem. Geol. 112, 179–191. https://doi.org/10.1016/0009-2541(94)90113-9.
Machado, J.P.S.L., Jelinek, A.R., Bicca, M.M., Stephenson, R., Genezini, F.A., 2019. West gondwana orogenies and pangaea break-up: Thermotectonic effects on the southernmost mantiqueira province, Brazil. J. Geol. Soc. Lond. 176, 1056–1075. https://doi.org/10.1144/jgs2019-018.
Machado, J.P.S.L., Jelinek, A.R., Stephenson, R., Gaucher, C., Bicca, M.M., Chiglino, L., Genezini, F.A., 2020. Low-temperature thermochronology of the South Atlantic margin along Uruguay and its relation to tectonic events in West Gondwana. Tectonophysics 784, 228439. https://doi.org/10.1016/j.tecto.2020.228439.
Machado, J.P., Jelinek, A.R., Stephenson, R., O'Sullivan, P., 2021a. Thermochronology of South America passive margin between Uruguay and southern Brazil: a lengthy and complex cooling history based on (U–Th)/he and fission tracks. J. S. Am. Earth Sci. 106, 103019 https://doi.org/10.1016/j.jsames.2020.103019.
Machado, J.P.S.L., Stephenson, R., Jelinek, A.R., Abdallah, R., 2021b. Sismoestratigrafia e evolução da Bacia de Pelotas. In: Jelinek, A.R., Sommer, C.A. (Eds.), Contribuições à Geologia Do Rio Grande Do Sul e de Santa Catarina. Editora Compasso, Porto Alegre, pp. 403–419. https://doi.org/10.29327/537860.1-24.
Martins-Ferreira, M.A.C., Dias, A.N.C., Chemale, F., Campos, J.E.G., 2020. Intracontinental uplift of the Brazilian Central Plateau linked to continental breakup, orogenies, and basin filling, supported by apatite and zircon fission-track data. Arab. J. Geosci. 13, 891. https://doi.org/10.1007/s12517-020-05885-8.
Milani, E.J., De Wit, M.J., 2014. Correlations between the classic Paraná and Cape-Karoo sequences of South America and southern Africa and their basin infills flanking the Gondwanides: Du Toit revisited. Geol. Soc. Spec. Publ. 294, 319–342. https://doi.org/10.1144/SP294.17.
Milani, E.J., Ramos, V.A., 1998. Paleozoic orogenies in southwestern Gondwana and the subsidence cycles of the Parana Basin. Rev. Bras. Geociências 28, 473–484.
Milani, E.J., Gonçalves De Melo, J.H., De Souza, P.A., Fernandes, L.A., França, A.B., 2007a. Bacia do paraná. Bol. Geoci. da Petrobras 15, 265–287.
Milani, E.J., Rangel, H.D., Bueno, G.V., Stica, J.M., Winter, W.R., Caixeta, J.M., Da Cruz Pessoa Neto, O., 2007b. Bacias sedimentares brasileiras - Cartas estratigráficas. Bol. Geoci. da Petrobras 15, 183–205.
Mohriak, W.U., 2004. Recursos energéticos associados à ativação tectônica mesozóica-cenozóica da América do Sul. In: Mantesso-Neto, V., Bartorelli, A., Carneiro, C.D.R., Brito-Neves, B.B. (Eds.), Geologia do Continente Sul-Americano: Evolução da obra de Fernando Flávio Marques de Almeida. Beca Produções Culturais Ltda, São Paulo, XVII, pp. 293–318.
Mohriak, W.U., Fainstein, R., 2012. Phanerozoic regional geology of the eastern Brazilian margin. In: Roberts, D.G., Bally, A.W. (Eds.), Regional Geology and Tectonics:

Phanerozoic Passive Margins, Cratonic Basins and Global Tectonic Maps. Elsevier, Boston, pp. 222–282. https://doi.org/10.1016/B978-0-444-56357-6.00006-8.
Mohriak, W., Nemčok, M., Enciso, G., 2008a. South Atlantic divergent margin evolution: Rift-border uplift and salt tectonics in the basins of SE Brazil. Geol. Soc. Spec. Publ. 294, 365–398. https://doi.org/10.1144/SP294.19.
Mohriak, W., Nemčok, M., Enciso, G., 2008b. South Atlantic divergent margin evolution: Rift-border uplift and salt tectonics in the basins of SE Brazil. Geol. Soc. Spec. Publ. 294, 365–398. https://doi.org/10.1144/SP294.19.
Mohriak, W.U., Nóbrega, M., Odegard, M.E., Gomes, B.S., Dickson, W.G., 2010. Geological and geophysical interpretation of the Rio Grande rise, south-eastern Brazilian margin: Extensional tectonics and rifting of continental and oceanic crusts. Pet. Geosci. 16, 231–245. https://doi.org/10.1144/1354-079309-910.
Moreira, J.L.P., Valdetaro, C.V., Gil, J.A., Machado, M.A.P., 2007. Bacia de Santos 2007. Bol. Geoci. da Petrobras 15, 531–549.
Moulin, M., Aslanian, D., Unternehr, P., 2010. A new starting point for the South and Equatorial Atlantic Ocean. Earth-Sci. Rev. 98, 1–37. https://doi.org/10.1016/j.earscirev.2009.08.001.
Murray, K.E., Orme, D.A., Reiners, P.W., 2014. Effects of U-Th-rich grain boundary phases on apatite helium ages. Chem. Geol. 390, 135–151. https://doi.org/10.1016/j.chemgeo.2014.09.023.
Nürnberg, D., Müller, R.D., 1991. The tectonic evolution of the South Atlantic from late Jurassic to present. Tectonophysics 191, 27–53. https://doi.org/10.1016/0040-1951(91)90231-G.
Oriolo, S., Oyhantçabal, P., Basei, M.A.S., Wemmer, K., Siegesmund, S., 2016. The Nico Pérez Terrane (Uruguay): from Archean crustal growth and connections with the Congo Craton to late Neoproterozoic accretion to the Río de la Plata Craton. Precambrian Res. 280, 147–160. https://doi.org/10.1016/j.precamres.2016.04.014.
Oriolo, S., Oyhantçabal, P., Wemmer, K., Siegesmund, S., 2017. Contemporaneous assembly of Western Gondwana and final Rodinia break-up: implications for the supercontinent cycle. Geosci. Front. 8, 1431–1445. https://doi.org/10.1016/j.gsf.2017.01.009.
Oyhantçabal, P., Siegesmund, S., Wemmer, K., Passchier, C.W., 2011. The transpressional connection between Dom Feliciano and Kaoko Belts at 580-550 Ma. Int. J. Earth Sci. 100, 379–390. https://doi.org/10.1007/s00531-010-0577-3.
Oyhantçabal, P., Cingolani, C.A., Wemmer, K., Siegesmund, S., 2018a. The Río de la Plata Craton of Argentina and Uruguay. In: Siegesmund, S., Basei, M.Â.S., Oyhantçabal, P., Oriolo, S. (Eds.), Geology of Southwest Gondwana. Springer, Cham, pp. 89–105. https://doi.org/10.1007/978-3-319-68920-3_4.
Oyhantçabal, P., Oriolo, S., Philipp, R.P., Wemmer, K., Siegesmund, S., 2018b. The Nico Pérez Terrane of Uruguay and Southeastern Brazil, Regional G. ed. In: Geology of Southwest Gondwana. Springer, Cham. https://doi.org/10.1007/978-3-319-68920-3_7.
Paim, P.S.G., Chemale Jr, F., Lopes, R. da C., 2000. A Bacia do Camaquã, in: Holz, M., De Ros, L.F. (Eds.), Geologia Do Rio Grande Do Sul. CIGO/UFRGS, Porto Alegre, pp. 231–274.
Passarelli, C.R., Stipp Basei, M.A., Siga, J.O., Hara, O.M.M., 2018. The Luis Alves and curitiba terranes: continental fragments in the adamastor ocean. In: Siegesmund, S., Basei, M.Â.S., Oyhantçabal, P., Oriolo, S. (Eds.), Geology of Southwest Gondwana. Springer, Cham, pp. 189–215. https://doi.org/10.1007/978-3-319-68920-3.
Philipp, R.P., Machado, R., 2005. The late Neoproterozoic granitoid magmatism of the Pelotas Batholith, southern Brazil. J. S. Am. Earth Sci. 19, 461–478. https://doi.org/10.1016/j.jsames.2005.06.010.
Philipp, R.P., Pimentel, M.M., Chemale, F., 2016. Tectonic evolution of the Dom Feliciano Belt in Southern Brazil: Geological relationships and U-Pb geochronology. Brazilian J. Geol. 46, 83–104. https://doi.org/10.1590/2317-4889201620150016.
Philipp, R.P., Pimentel, M.M., Basei, M.A.S., 2018. The tectonic evolution of the são gabriel terrane, Dom Feliciano Belt, Southern Brazil: the closure of the Charrua Ocean. In: Siegesmund, S., Basei, M.Â.S., Oyhantçabal, P., Oriolo, S. (Eds.), Geology of Southwest Gondwana. Springer, Cham, pp. 243–265. https://doi.org/10.1007/978-3-319-68920-3_10.
Price, P.B., Walker, R.M., 1963. Fossil tracks of charged particles in mica and the age of minerals. J. Geophys. Res. 68, 4847–4862. https://doi.org/10.1029/JZ068i016p04847.
Rabinowitz, P.D., Labrecque, J., 1979. The Mesozoic South Atlantic Ocean and evolution of its continental margins. J. Geophys. Res. 84, 5973–6002. https://doi.org/10.1029/JB084iB11p05973.
Reiners, P.W., Farley, K.A., 2001. Influence of crystal size on apatite (U-Th)/He thermochronology: an example from the Bighorn Mountains, Wyoming. Earth Planet. Sci. Lett. 188, 413–420. https://doi.org/10.1016/S0012-821X(01)00341-7.
Reiners, P.W., Carlson, R.W., Renne, P.R., Cooper, K.M., Granger, D.E., McLean, N.M., Schoene, B., 2017. Geochronology and Thermochronology. Wiley-Blackwell. https://doi.org/10.1002/9781118455876.
Riccomini, C., Velázquez, V.F., Gomes, C.B., 2005. Tectonic controls of the Mesozoic and Cenozoic alkaline magmatism in the central- southeastern Brazilian Platform. Mesozoic to Cenozoic Alkaline Magmat. Brazilian Platf. 31–57.
Shuster, D.L., Flowers, R.M., Farley, K.A., 2006. The influence of natural radiation damage on helium diffusion kinetics in apatite. Earth Planet. Sci. Lett. 249, 148–161. https://doi.org/10.1016/j.epsl.2006.07.028.
Sonoki, I.K., Garda, G.M., 1988. Idades K-Ar de rochas alcalinas do Brasil meridional e Paraguai oriental: compilação e adaptação às novas constantes de decaimento. Bol. IG-USP. Série Científica 19, 63–85. https://doi.org/10.11606/issn.2316-8986.v19i0p63-85.
Spiegel, C., Kohn, B., Belton, D., Berner, Z., Gleadow, A., 2009. Apatite (U-Th-Sm)/he thermochronology of rapidly cooled samples: the effect of he implantation. Earth Planet. Sci. Lett. 285, 105–114. https://doi.org/10.1016/j.epsl.2009.05.045.
Stewart, K., Turner, S., Kelley, S., Hawkesworth, C., Kirstein, L., Mantovani, M., 1996. 3-D, 40Ar-39Ar geochronology in the Paraná continental flood basalt province. Earth Planet. Sci. Lett. 143, 95–109. https://doi.org/10.1016/0012-821x(96)00132-x.
Stockli, D.F., Farley, K.A., Dumitru, T.A., 2000. Calibration of the apatite (U-Th)/he thermochronometer on anexhumed fault block, White Mountains, California. Geology 28, 983–986. https://doi.org/10.1130/0091-7613(2000)28<983:COTAHT>2.0.CO;2.
Tagami, T., O'Sullivan, P.B., 2005. Fundamentals of fission-track thermochronology. Rev. Mineral. Geochem. 58, 19–47. https://doi.org/10.2138/rmg.2005.58.2.
Talwani, M., Abreu, V., 2000. Inferences regarding initiation of oceanic crust formation from the U.S. east coast margin and conjugate South Atlantic margins. In: Mohriak, W.U., Talwani, M. (Eds.), Atlantic Rifts and Continental Margins. American Geophysical Union, Washington, p. 115. https://doi.org/10.1029/GM115p0211.
Torsvik, T.H., Rousse, S., Labails, C., Smethurst, M.A., 2009. A new scheme for the opening of the South Atlantic Ocean and the dissection of an Aptian salt basin. Geophys. J. Int. 177, 1315–1333. https://doi.org/10.1111/j.1365-246X.2009.04137.x.
Turner, S., Regelous, M., Kelley, S., Hawkesworth, C., Mantovani, M., 1994. Magmatism and continental break-up in the South Atlantic: high precision 40Ar39Ar geochronology. Earth Planet. Sci. Lett. 121, 333–348. https://doi.org/10.1016/0012-821X(94)90076-0.
Vermeesch, P., 2009. RadialPlotter: a Java application for fission track, luminescence and other radial plots. Radiat. Meas. 44, 409–410. https://doi.org/10.1016/j.radmeas.2009.05.003.
Wildner, W., Camozzato, E., Toniolo, J.A., Binotto, R.B., Iglesias, C.M.F., Laux, J.H., 2014. Mapa geológico do Estado de Santa Catarina. In: Porto Alegre: CPRM. Escala 1: 500.000. Programa Geologia do Brasil. Subprograma de Cartografia Geológica Regional.
Wolf, R.A., Farley, K.A., Silver, L.T., 1996. Helium diffusion and low-temperature thermochronometry of apatite. Geochim. Cosmochim. Acta 60, 4231–4240. https://doi.org/10.1016/S0016-7037(96)00192-5.
Wolf, R.A., Farley, K.A., Kass, D.M., 1998. Modeling of the temperature sensitivity of the apatite (U-Th)/he thermochronometer. Chem. Geol. 148, 105–114. https://doi.org/10.1016/S0009-2541(98)00024-2.